Solid State and Solution Characterization of Copper and Cobalt Complexes with Amide and Thioamide Ligands

By

James B. Mills

Submitted to the graduate degree program in Chemistry and the Graduate Faculty of the University of Kansas in partial fulfillment of the requirements for the degree of Master of Science.

_____

Chairperson Dr. Timothy A. Jackson, Ph.D.

_____

Dr. Kristin Bowman-James, Ph.D.

_____

Dr. Mikhail V. Barybin, Ph.D.

Date Defended: 6/20/12

The Thesis Committee for James B. Mills

certifies that this is the approved version of the following thesis:

Solid State and Solution Characterization of Copper and Cobalt Complexes

with Amide and Thioamide Ligands

_____

Chairperson Dr. Timothy A. Jackson, Ph.D.

Date approved: 8/2/12

Abstract

Low molecular weight ligands have been extremely useful for mimicking active intermediates. While often times these low molecular weight compounds are synthesized with ligands that do not always fully mirror the active site, they do hold an advantage over studying intermediates of full proteins due to the complexity of an entire protein. This work utilizes biologically relevant amide groups to explore biomimetic copper chemistry. The amide functional group is found in all biological systems because it forms the peptide backbone. The amide complexes synthesized were studied in terms of electronic ground states, as well as reactivity with biologically relevant oxidants. One dicopper (II:II) amide macrocyclic complex was synthesized and characterized and has shown that the copper centers couple in a ferromagnetic manner. This complex also showed a significant change in the UV-vis spectrum in the presence of potassium superoxide. In future work, this could lend insight into the role and function of prion protein (PrP), a multinuclear copper protein, whose function is still debated in the literature.

Abbreviations:

EPR	electron paramagnetic resonance
ENDOR	electron nuclear double resonance
IR	infrared
MCD	magnetic circular dichroism
NMR	nuclear magnetic resonance
SNS_{Phenyl}	N^2,N^6-bis(phenyl)pyridine-2,6-dithiicarboxamide
$SNS_{t\text{-}butyl}$	N^2,N^6-bis(t-butyl)pyridine-2,6-dithiicarboxamide
NNN_{Phenyl}	N^2,N^6-bis(phenyl)pyridine-2,6-dicarboxamide
SOMO	singly occupied molecular orbital
VTVH	variable-temperature, variable-field

Copper Containing Proteins

Chapter 1

1.1 Motivation

Copper proteins are able to perform essential roles in biological systems from mollusks to mammals. It is clear that utilizing copper as a redox active metal allows for many vital biological functions from defense against free radicals to pigmentation. Studying the protein in its entirety is a necessity in order to further our knowledge of these systems. The characterization and isolation of active intermediates proves extremely difficult due to the large size and complexity of these proteins and the instability of the intermediates. To this end low molecular weight models are necessary to simplify our view to the active site alone. Therefore the goal of this research is to synthesize and characterize such complexes to lend insight into possible mechanisms and functions of copper metalloproteins. The complexes in this work were synthesized utilizing biologically relevant amide based ligands. Amides are a functional group that are utilized in the backbone of proteins making this functional group relevant in low molecular weight compounds to mimic biological systems.

1.2 Introduction

Copper cofactors in metalloenzymes have been studied extensively and have been shown to catalyze many redox reactions as well as perform oxygen transport. These proteins have not only been studied by x-ray diffraction but also using a variety of spectroscopic techniques including electon paramagnetic resonance (EPR), x-ray absorption, resonance raman, UV-vis absorption, and magnetic circular dichroism (MCD). The active sites of these proteins can contain a number of copper centers, from one up to four, as is the case with nitrous oxide

reductase. The numbers of functions that these sites can perform are vast and include electron-transfer,[1-4] oxidation of organic substrates,[2,5-16] disproportionation of superoxide,[17,18] and reduction of nitrite and nitrous oxide.[1,4,19-21] This chapter focuses on four proteins in particular: tyrosinase, catechol oxidase, nitrous oxide reductase, and prion protein. These proteins were chosen because they contain multiple metal centers that allow them to achieve their biological function. For comparison the metalloprotein hemocyanin will be explored due to the identical copper active site as tyrosinase and catechol oxidase. Unlike tyrosinase and catechol oxidase, which are involved in oxygen activation, hemocyanin is an oxygen transport protein.

1.3 Dinuclear copper metalloproteins

Active sites that contain two copper centers are very common in biological systems and allow for a broad array of functions such as electron transfer, oxidation, and oxygen transport. Two possible reaction pathways in enzymes containing two metal center are a two electron oxidation of a tyrosine residue to an *o*-catechol, or a two electron oxidation of a *o*-catechol to an *o*-quinone (Scheme 1.1).[22] Evidence of this oxidation is apparent when an apple is cut and the inside is exposed to oxygen; the apple turns brown. Another example is when humans are exposed to sun, and in turn their skin is darkened. In fact lack of tyrosinase is one of the causes of albinism in mammals. There is still some debate in the literature as to what species is the active oxidant for tyrosinase oxidation. It is possible for molecular oxygen to oxidize the metal centers leading to a bridging peroxo leaving the coppers in a divalent state or the oxygen can

further oxidize the centers to Cu(III) leading to a bis-μ-oxo complex. It has been shown in small molecule mimics, both theoretically and experimentally, that these states interconvert because there is virtually no energy required for rearrangement as the metal binding site of both species change very minimally.[23-27] Both of these species have been characterized in small molecule systems but the active oxidant of the enzyme is still debated. To further peroxo species have O-O bond distances of 1.41 Å while the bis-μ-oxo have an O-O distance of 2.35 Å.

Scheme 1.1

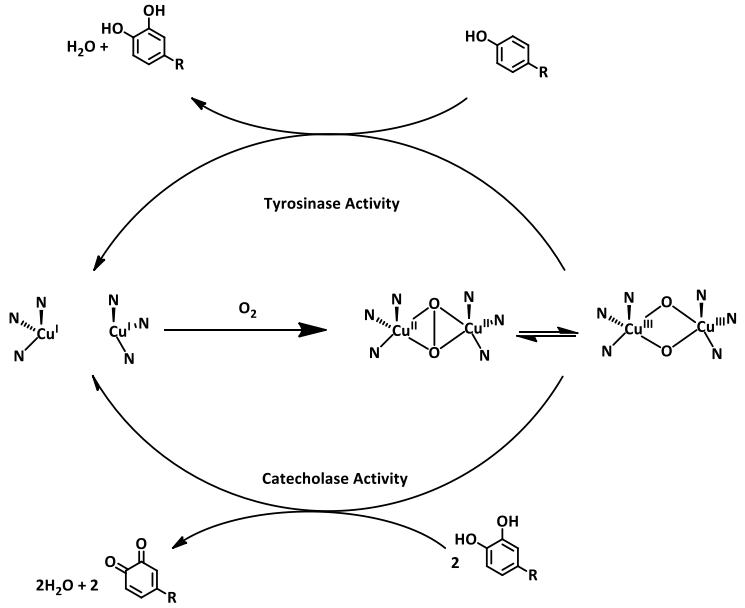

Interestingly, the two enzymes share an identical active site with the metalloprotein hemocyanin, which shows no enzymatic activity and is utilized for oxygen transport in mollusks, comparable to hemoglobin in mammals.[5,28] The active sites of catechol oxidase, tyrosinase, and deoxyhemocyanin are virtually identical (Figures 1.1, 1.2, and 1.3).[5,12,29,30] The primary difference in the three structures is the bridging hydroxide found in catechol oxidase and tyrosinase. This hydroxide bridge can account for the vastly decreased Cu-Cu distance. In

hemocyanin the lack of a bridging hydroxide gives a Cu-Cu distance of 4.6 Å while the catechol oxidase has a Cu-Cu distance of 2.9 Å. Hemocyanin, being an oxygen transport protein allows the oxygen bound form to be more stable allowing researchers to obtain a crystal structure of the dioxygen bound form (Figure 1.4).[5] The oxygen bound form of hemocyanin lends insight into the manner in which oxygen is bound as well as the oxidation state of the copper ions.

The oxygen gets reduced to a peroxide dianion and is bound in a μ-η^2:η^2 fashion with a Cu-Cu distance decreased by one angstrom to 3.6 Å. Researchers have been able to utilize x-ray absorption for an intermediate of catechol oxidase which indicates a similar binding mode of oxygen and a Cu-Cu distance of 3.8 Å.[12,29] In 2006, Sugiyama and coworkers isolated a crystal suitable for x-ray diffraction and thus obtained a structure of an oxygen bound form of tyrosinase which shows the oxygen bound as a peroxide and a Cu-Cu distance of 3.45 Å, slightly shorter then the Cu-Cu distance in hemocyanin(Figure 1.5).[30] Interestingly, although the active sites of hemocyanin, tyrosinase, and catechol oxidase are basically superimposable, the amino acid sequences only show ~20% similarity. It has also been shown that the difference in the reactivity of the proteins stems from the position of the active site either on the periphery (tyrosinase and catechol oxidase) or the interior (hemocyanin) of the protein. The location of the active site relative to other metal ion sites is also important in multinuclear copper enzymes such as nitrous oxide reductase.

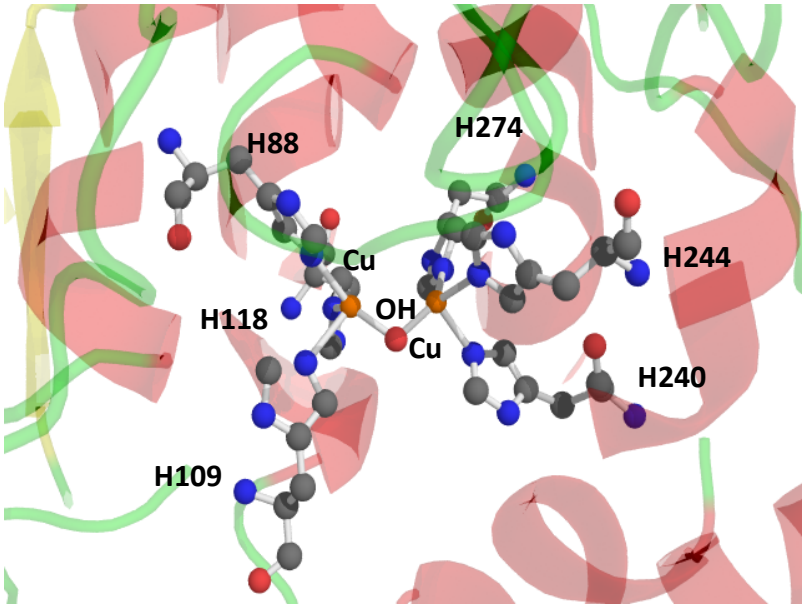

Figure 1.1: Active site of catechol oxidase from Protein Data Bank (pdb) file 1BT3

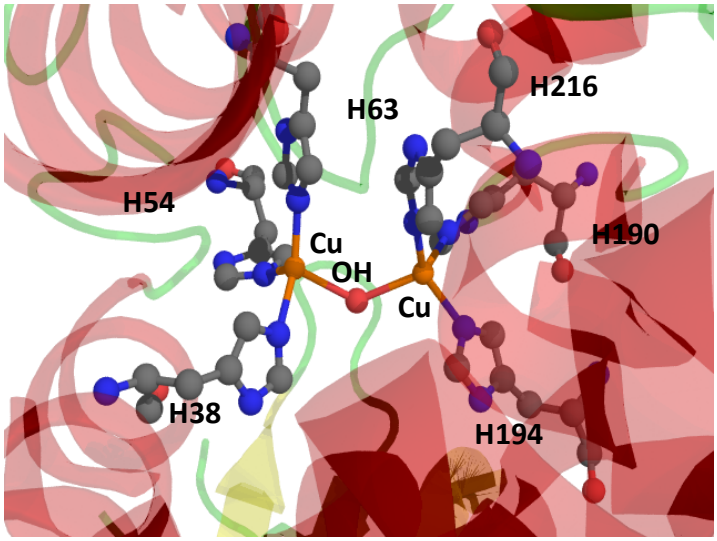

Figure 1.2: Active site of tyrosinase (pdb file 1WX5)

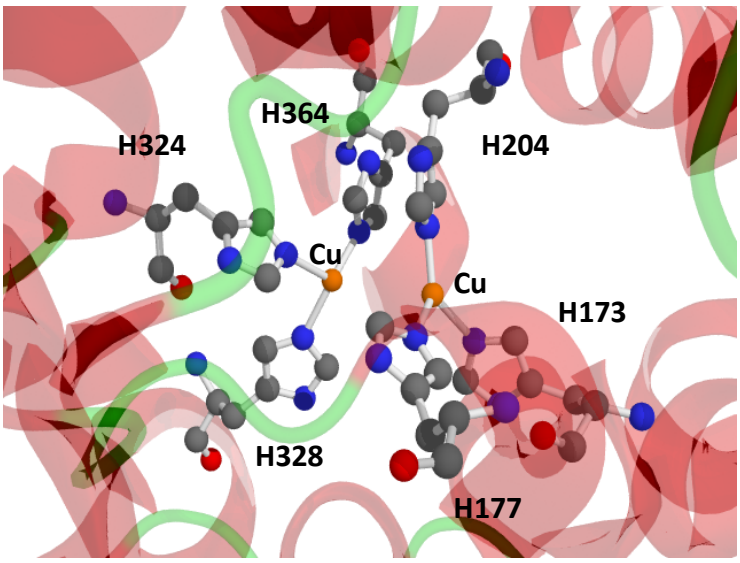

Figure 1.3: Active site of deoxyhemocyanin (pdb file 1LLA)

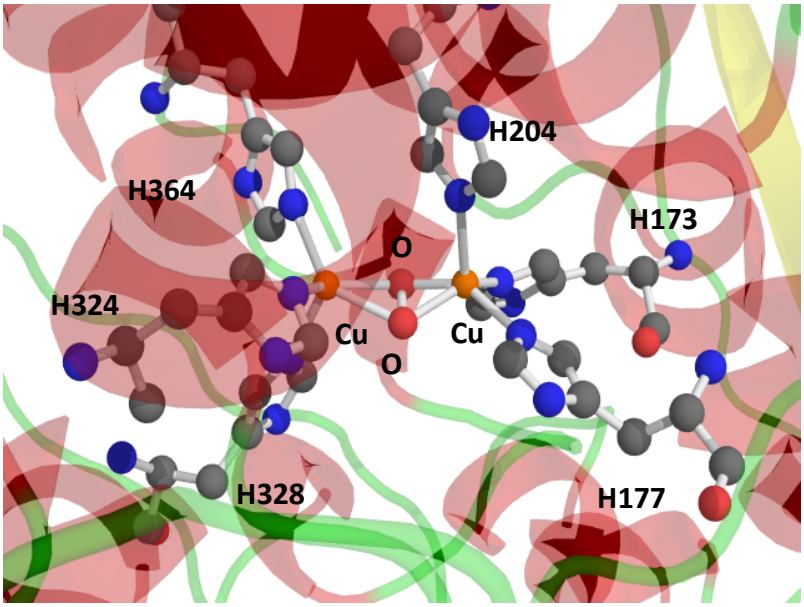

Figure 1.4: Active site of oxyhemocyanin (pdb file 1OXY)

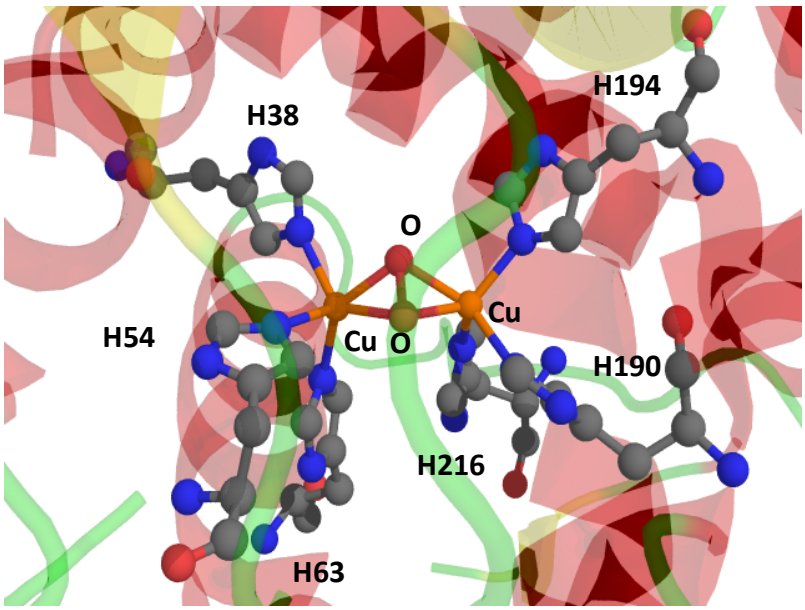

Figure 1.5: Active site of oxytyrosinase (pdb file 1WX4)

1.4 Multi-copper Enzymes

Multinuclear copper active sites, with greater than two copper ions have been studied in detail as well. Nitrous oxide reductase performs reduction of nitrous oxide to molecular nitrogen also yielding water as opposed to the previously discussed oxidation chemistry. The active site of this protein contains copper metal centers bridged through a sulfur atom as seen by X-ray diffraction of a crystal from Cambillau and co-workers (Figure 1.6).[4] Spectroscopic characterization by Neese and co-workers indicated a second metal site similar to the purple copper site in cytochrome c oxidase which contains two coppers not near the active site. This finding was confirmed in a crystal structure from Michel and co-workers.[31,32] The so-called purple copper site, which is characterized by intense sulfur to metal charge transfer transitions at 480 nm and 530 nm and unusually small hyperfine coupling in the EPR spectrum, has been

shown to perform electron transport to the active site.[32,33] The x-ray structure of nitrous oxide reductase (solved in 2000) confirmed this finding, showing a fifth and sixth copper ions 11 Å from the active site which are utilized for electron transfer (Figure 1.7).[4] In 2004 Solomon and co-workers performed experiments to further characterize the active site.[1] Based upon EPR data it was shown that in the resting state of the protein, the active site contains a mixed valent system with three Cu(I) ions and a Cu(II) ion. Upon activation, the EPR signal disappeared indicating that the paramagnetic Cu(II) ion was reduced to diamagnetic Cu(I). The proposed reaction scheme is shown with the source of the electrons being the purple copper site which continuously gets reduced by an external electron source (Scheme 1.2).[34]

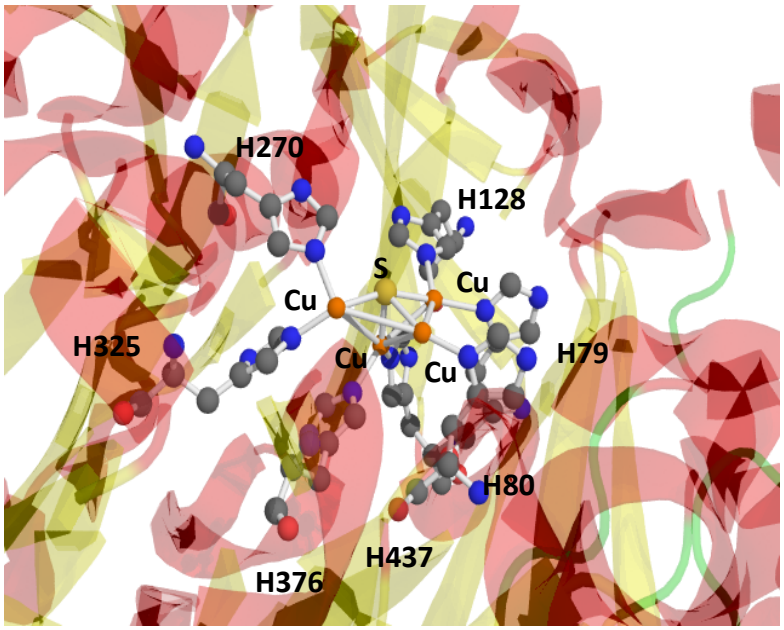

Figure 1.6: Active site nitrous oxide reductase (pdb 1FWX)

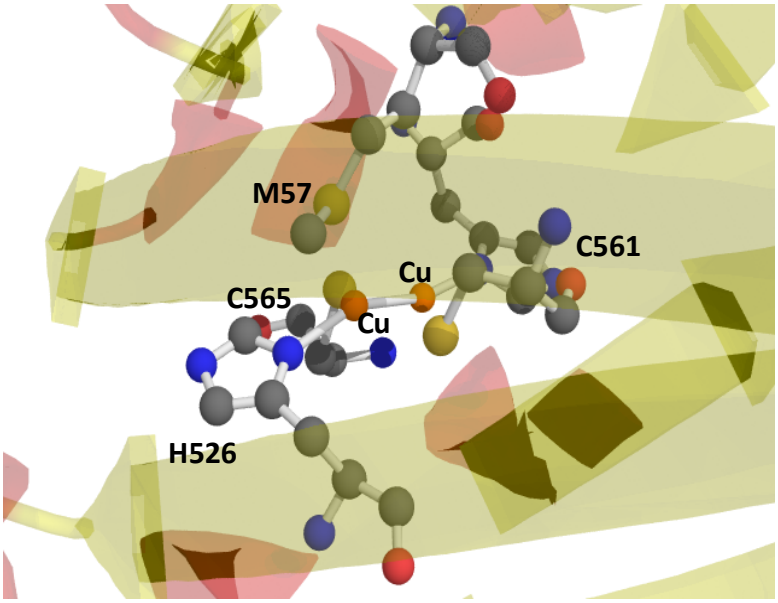

Figure 1.7: Purple copper site in nitrous oxide reductase (pdb 1FWX)

Scheme 1.2: Proposed reaction scheme for nitrous oxide reductase (adapted from [35] and [34])

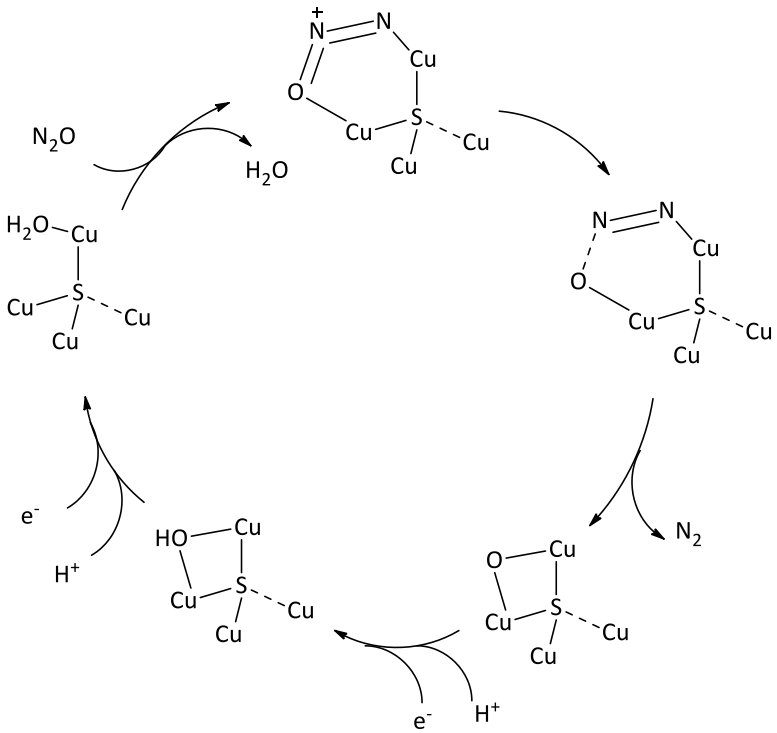

While the function of nitrous oxide reductase is well documented, there is another multicopper enzyme, prion protein (PrP) whose function is still being debated. PrP is a copper containing protein present in the central nervous system and in certain cases the protein can misfold and aggregate causing so called prion diseases including Creutzfeldt-Jakob disease in humans and "mad cow" in cattle which causes neurodegeneration similar to Alzheimer's disease. In 1997 Stanley B. Prusiner was awarded the Nobel Prize in Physiology or Medicine for his work with PrP. In more recent literature the function of prion protein has been debated among many experts in the field.[36-41] In PrP copper can bind in two separate ways depending upon concentration of metal in the environment. Binding of a metal ion occurs in the so-called octarepeat region of the protein which occurs at the extremely flexible N-terminus. The repeat sequence (PHGGGWQ) in human PrP is repeated four times. This region contains four total histidines, which in low copper concentration all bind to the four coordinated Cu(II) according to electron nuclear double resonance (ENDOR) EPR studies examining the hyperfine coupling.[37,38,42] Based upon EPR data it is known that if copper concentration exists in excess of a 1:1 Cu:PrP ratio, the binding includes only one histidine per metal as well as two deprotonated amide nitrogens from the backbone and an amide oxygen.[43,44] The latter binding mode is pH dependent. In acidic conditions the amides reprotonate causing these two ligating atoms to dissociate.[45] While the binding mode of the copper centers in PrP has been characterized, the function of the protein is still under debate. Some groups believe that PrP plays a critical role in Cu(II) regulation in areas of high concentration of the metal ion to prevent the free ion from aiding in the formation of reactive oxygen species.[36-39,46-48] Others contend that the bound Cu(II) assists in the disproportionation of superoxide to hydrogen peroxide, but

studies continue with PrP to definitively identify its function. [36-41] The complexity of the PrP, in particular the flexibility of the metal binding site, makes characterization difficult so often research is performed on fragments of the protein. Another possible solution is to utilize small molecule mimics in order to aid in exploring possible functionality.

References:

(1) Chen, P.; Gorelsky, S. I.; Ghosh, S.; Solomon, E. I. *Angewandte Chemie-International Edition* **2004**, *43*, 4132.

(2) Ito, N.; Phillips, S. E. V.; Stevens, C.; Ogel, Z. B.; McPherson, M. J.; Keen, J. N.; Yadav, K. D. S.; Knowles, P. F. *Nature* **1991**, *350*, 87.

(3) Colman, P. M.; Freeman, H. C.; Guss, J. M.; Murata, M.; Norris, V. A.; Ramshaw, J. A. M.; Venkatappa, M. P. *Nature* **1978**, *272*, 319.

(4) Brown, K.; Djinovic-Carugo, K.; Haltia, T.; Cabrito, I.; Saraste, M.; Moura, J. J. G.; Moura, I.; Tegoni, M.; Cambillau, C. *Journal of Biological Chemistry* **2000**, *275*, 41133.

(5) Magnus, K. A.; Hazes, B.; Tonthat, H.; Bonaventura, C.; Bonaventura, J.; Hol, W. G. J. *Proteins-Structure Function and Genetics* **1994**, *19*, 302.

(6) Solomon, E. I.; Chen, P.; Metz, M.; Lee, S. K.; Palmer, A. E. *Angewandte Chemie-International Edition* **2001**, *40*, 4570.

(7) Prigge, S. T.; Kolhekar, A. S.; Eipper, B. A.; Mains, R. E.; Amzel, L. M. *Science* **1997**, *278*, 1300.

(8) Prigge, S. T.; Eipper, B. A.; Mains, R. E.; Amzel, L. M. *Science (Washington, DC, U. S.)* **2004**, *304*, 864.

(9) Lieberman, R. L.; Rosenzweig, A. C. *Nature (London, U. K.)* **2005**, *434*, 177.

(10) Steiner, R. A.; Kalk, K. H.; Dijkstra, B. W. *Proc. Natl. Acad. Sci. U. S. A.* **2002**, *99*, 16625.

(11) Steiner, R. A.; Meyer-Klaucke, W.; Dijkstra, B. W. *Biochemistry* **2002**, *41*, 7963.

(12) Klabunde, T.; Eicken, C.; Sacchettini, J. C.; Krebs, B. *Nature Structural Biology* **1998**, *5*, 1084.

(13) Messerschmidt, A.; Rossi, A.; Ladenstein, R.; Huber, R.; Bolognesi, M.; Gatti, G.; Marchesini, A.; Petruzzelli, R.; Finazzi-Agro, A. *J. Mol. Biol.* **1989**, *206*, 513.

(14) Lindley, P. F.; Card, G.; Zaitseva, I.; Zaitsev, V.; Reinhammar, B.; Selin-Lindgren, E.; Yoshida, K. *JBIC, J. Biol. Inorg. Chem.* **1997**, *2*, 454.

(15) Whittaker, J. W. *Chemical Reviews* **2003**, *103*, 2347.

(16) Kim, E.; Chufan, E. E.; Kamaraj, K.; Karlin, K. D. *Chemical Reviews* **2004**, *104*, 1077.

(17) Bertini, I.; Mangani, S.; Viezzoli, M. S. *Advances in Inorganic Chemistry, Vol 45* **1998**, *45*, 127.

(18) Tolman, W. B., Ed.; Elsevier Ltd.: Oxford, 2004; Vol. 8.

(19) Wasser, I. M.; de, V. S.; Moeenne-Loccoz, P.; Schroeder, I.; Karlin, K. D. *Chem. Rev. (Washington, D. C.)* **2002**, *102*, 1201.

(20) Fenderson, F. F.; Kumar, S.; Adman, E. T.; Liu, M. Y.; Payne, W. J.; LeGall, J. *Biochemistry* **1991**, *30*, 7180.

(21) Godden, J. W.; Turley, S.; Teller, D. C.; Adman, E. T.; Liu, M. Y.; Payne, W. J.; LeGall, J. *Science (Washington, D. C., 1883-)* **1991**, *253*, 438.

(22) *Concepts and Models in Bioinorganic Chemistry*; Heinz-Bernard Kraatz, N. M.-N., Ed.; Wiley-VCH: Weinheim, 2006.

(23) Lewis, E. A.; Tolman, W. B. *Chemical Reviews* **2004**, *104*, 1047.

(24) Mirica, L. M.; Ottenwaelder, X.; Stack, T. D. P. *Chemical Reviews* **2004**, *104*, 1013.

(25) Pidcock, E.; Obias, H. V.; Abe, M.; Liang, H. C.; Karlin, K. D.; Solomon, E. I. *Journal of the American Chemical Society* **1999**, *121*, 1299.

(26) Que, L. Jr.; Tolman, W. B. *Angewandte Chemie-International Edition* **2002**, *41*, 1114.

(27) Pidcock, E.; Obias, H. V.; Zhang, C. X.; Karlin, K. D.; Solomon, E. I. *Journal of the American Chemical Society* **1998**, *120*, 7841.

(28) Solomon, E. I.; Sundaram, U. M.; Machonkin, T. E. *Chemical Reviews* **1996**, *96*, 2563.

(29) Eicken, C.; Zippel, F.; Buldt-Karentzopoulos, K.; Krebs, B. *Febs Letters* **1998**, *436*, 293.

(30) Matoba, Y.; Kumagai, T.; Yamamoto, A.; Yoshitsu, H.; Sugiyama, M. *Journal of Biological Chemistry* **2006**, *281*, 8981.

(31) Ostermeier, C.; Iwata, S.; Ludwig, B.; Michel, H. *Nature Structural Biology* **1995**, *2*, 842.

(32) Neese, F.; Zumft, W. G.; Antholine, W. E.; Kroneck, P. M. H. *Journal of the American Chemical Society* **1996**, *118*, 8692.

(33) Williams, K. R.; Gamelin, D. R.; LaCroix, L. B.; Houser, R. P.; Tolman, W. B.; Mulder, T. C.; deVries, S.; Hedman, B.; Hodgson, K. O.; Solomon, E. I. *Journal of the American Chemical Society* **1997**, *119*, 613.

(34) Tavares, P.; Pereira, A. S.; Moura, J. J. G.; Moura, I. *Journal of Inorganic Biochemistry* **2006**, *100*, 2087.

(35) Gorelsky, S. I.; Ghosh, S.; Solomon, E. I. *Journal of the American Chemical Society* **2006**, *128*, 278.

(36) Gaggelli, E.; Kozlowski, H.; Valensin, D.; Valensin, G. *Chemical Reviews* **2006**, *106*, 1995.

(37) Millhauser, G. L. *Accounts of Chemical Research* **2004**, *37*, 79.

(38) Millhauser, G. L. In *Annual Review of Physical Chemistry* 2007; Vol. 58, p 299.

(39) Singh, N.; Singh, A.; Das, D.; Mohan, M. L. *Antioxidants & Redox Signaling* **2010**, *12*, 1271.

(40) Vassallo, N.; Herms, J. *Journal of Neurochemistry* **2003**, *86*, 538.

(41) Liu, L.; Jiang, D. L.; McDonald, A.; Hao, Y. Q.; Millhauser, G. L.; Zhou, F. M. *Journal of the American Chemical Society* **2011**, *133*, 12229.

(42) Davies, P.; Brown, D. R. *Biochemical Journal* **2008**, *410*, 237.

(43) Chattopadhyay, M.; Walter, E. D.; Newell, D. J.; Jackson, P. J.; Aronoff-Spencer, E.; Peisach, J.; Gerfen, G. J.; Bennett, B.; Antholine, W. E.; Millhauser, G. L. *Journal of the American Chemical Society* **2005**, *127*, 12647.

(44) Walter, E. D.; Chattopadhyay, M.; Millhauser, G. L. *Biochemistry* **2006**, *45*, 13083.

(45) Davies, P.; Marken, F.; Salter, S.; Brown, D. R. *Biochemistry* **2009**, *48*, 2610.

(46) Kozlowski, H.; Janicka-Klos, A.; Brasun, J.; Gaggelli, E.; Valensin, D.; Valensin, G. *Coordination Chemistry Reviews* **2009**, *253*, 2665.

(47) Koppenol, W. H. *Redox Report* **2001**, *6*, 339.

(48) Baruch-Suchodolsky, R.; Fischer, B. *Biochemistry* **2009**, *48*, 4354.

Structural and Spectroscopic Characterization of SNS Thioamide Pincer Cu(II) Complexes

Chapter 2

2.1 Introduction

Pincer complexes are used for a variety of purposes such as C-C bond activation, alkane dehydrogenation, gas sensing, among many others.[1-3] Pincers were initially defined as tridentate ligands bound through a central anionic carbon of an aromatic ring and two side chains with electron donating atoms such as nitrogen, sulfur or phosphorus (Figure 2.1),

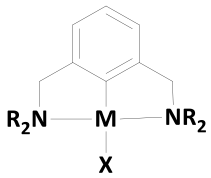

Figure 2.1: Representation of a pincer ligand[4]

although more recently pincers with the central atom being nitrogen have been explored.[4-10] The chemistry of pincer ligands began by focusing on precious metals, although some work has been done on first row transition metals.[11,12]

In 2004, and subsequently in 2006, the Bowman-James group successfully synthesized a group of thioamide complexes with palladium.[13,14] The pincer ligand shown below is proven to have interesting acid/base chemistry (Scheme 2.1). These ligands have the ability to lose either

Scheme 2.1

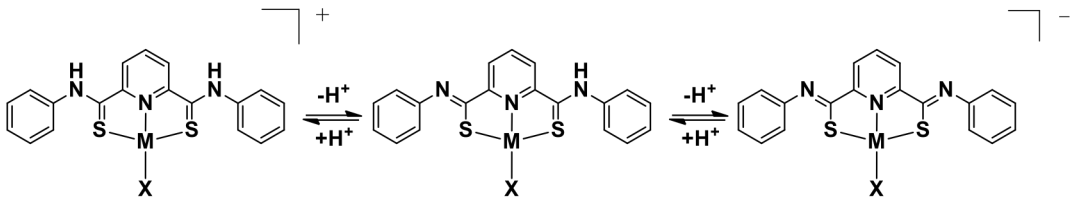

a single proton forming a mixed thioamide/iminothiolate complex. When the complex loses two protons, the diiminothiolate complex is formed. This allows for charge versatility of the ligand, therefore altering the ligand bound at the fourth coordination site.

In subsequent years, Kanbara and co-workers investigated this phenomenon in more detail exploring the stepwise deprotonation events in solution with a variety of metals such as nickel, ruthenium, and palladium.[15-19] Aside from crystallographic evidence, other methods such as NMR, UV-vis absorption, and cyclic voltammetry (CV) can be utilized in the characterization of these complexes as seen in 2011. The complex below with a meta-xylyl phenyl-dithiocarboxamide was synthesized and characterized (Figure 2.2).[18] Other complexes containing a pyrole substituted for the meta-xylyl were also used. The cyclic voltammetry studies were performed as the number of equivalents of base increased, and as the equivalents of base increased, the redox potential increased as well. This due to the anionic nature of the

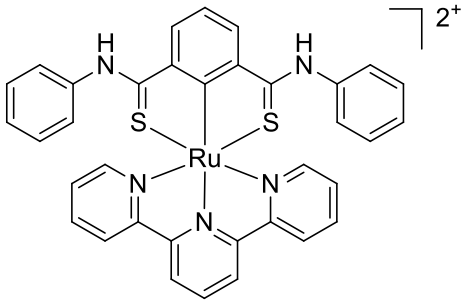

Figure 2.2: Ruthenium complex synthesized and characterized by Kanbara to explore effect of deprotonation on reduction potentials.

thiolate moiety upon deprotonation of the nitrogen. The first deprotonation event could be achieved with the use of the relatively weak base (triethylamine with a pKa of the conjugate

acid of 10.75). The second deprotonation requires a stronger base (DBU(1,8-diazabicycloundec-7-ene) with a pKa of the conjugate acid of 12). As mentioned previously, the deprotonation can alter the nature of the ligand at the fourth coordination site to accommodate the preferred neutral complex.

In recent literature, the ability to tune the ligand while in solution has afforded uses as a switch for the binding and release of a desired substrate. In 2012, Bowman-James and coworkers reported a bound mustard surrogate 2-chloroethyl ethyl sulfide (CEES) upon deprotonation of the complexes.[20] Initially, the complex is seen to be either singly deprotonated and a bind chloride in the fourth coordination site for a neutral complex. Alternatively, when the ligand is doubly deprotonated a neutral ligand is found at the fourth coordination site to make a neutral complex. The authors were also able to show that this switch in coordination is reversible. Upon the addition of an acid, the species reverted back to the chloride bound species. This reversible binding has many possible applications including pharmacological, sensing, and sequestration; although, due to the expense of the metals previously used, a cheaper alternative would be ideal.

In 2011 Kanbara and co-workers showed precedence for binding copper into similar thioamide ligands. It was seen that when using copper chloride, the copper was arranged in a similar manner as the platinum complex from the Bowman-James group. The complex formed a dimer bridging through the sulfur on the iminothiolate to put the copper in a square pyramidal geometry, although the acid/base chemistry was not explored.[16]

2.2 Ligands and Complexes Discussed in this Chapter

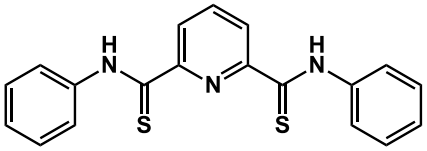

SNS_{Phenyl}

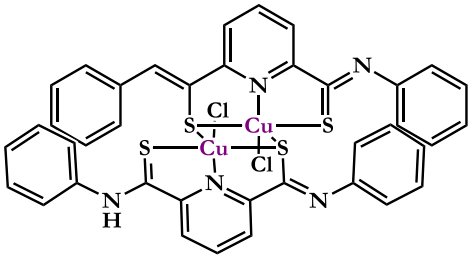

$[Cu(SNS_{Phenyl})Cl]_2$

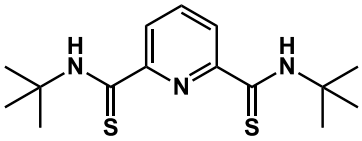

$SNS_{t\text{-}butyl}$

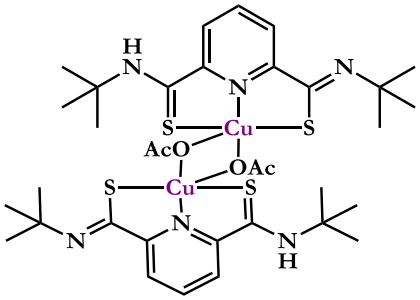

$[Cu(SNS_{t\text{-}butyl})OAc]_2$

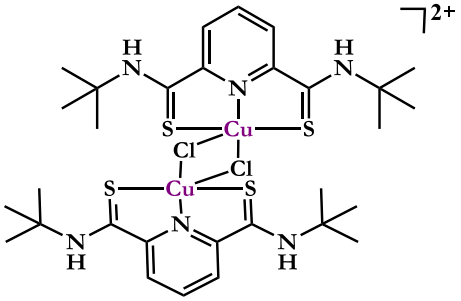

$[Cu(SNS_{t\text{-}butyl})Cl]_2$

2.3 Results and Discussion

2.3.1 $[Cu(SNS_{Phenyl})Cl]$

In order to explore the acid/base chemistry for a paramagnetic transition metal, a series of thioamide complexes with copper was synthesized.[15] The $[Cu^{II}(SNS_{Phenyl})Cl]_2$ structure, unlike the Pt counterpart, is mono-deprotonated which allows the structure to be neutral in the solid state forming a dimeric complex through a bridging thiolate (Figure 2.3). The apical $S_{thiolate}$ - Cu distance is long at 2.971 Å leading to a square pyramidal geometry allowing for a Cu-Cu distance of 3.59 Å (Table 2.1).

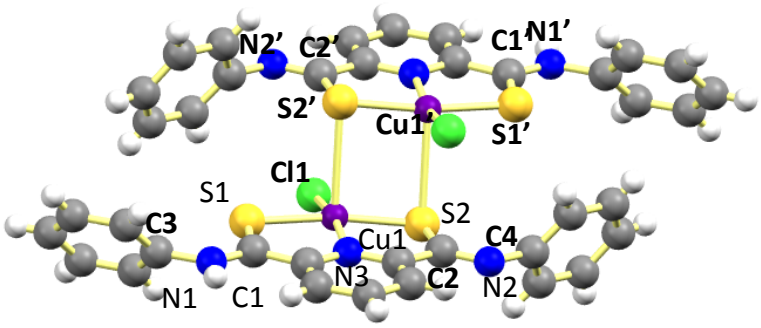

Figure 2.3: Crystal structure of $[Cu(SNSPhenyl)Cl]_2$

Table 2.1: $[Cu^{II}(SNS_{Phenyl})Cl]_2$

Selected Bond Lengths (Å)		Selected Bond Angles (deg)	
Cu1-S1	2.2648(6)	C1-N1-C3	126.40(18)
Cu1-S2	2.2454(6)	C2-N2-C4	119.53(18)
Cu1-Cl1	2.2552(6)	Cu1-S2_Cu1'	85.82
Cu1-N3	1.9865(2)		
Cu1-S2'	2.971(0)		
S1-C1	1.681(2)		
C1-N1	1.326(3)		
C2-N2	1.280(3)		
S2-C2	1.760(2)		

The copper sits 0.17 Å out of the plane of the base of the pyramid toward the bridging thiolate on the adjacent ligand (Figure 2.4). To further confirm that the ligand is mono-deprotonated, the C1-N1 distance of 1.33 Å compared to 1.27 Å for C2-N2 indicates that C1-N1 has more single bond character than C2-N2. The C1-S1 and C2-S2 distances which are 1.68 Å and 1.76 Å respectively, also indicate that the former has more double bond character. The C1-N1 and C1-S1 distances compare well with Cu(II) complexes synthesized in 2007 by Corbella and co-workers in which they used a tertiary thioamide that does not have the ability to undergo deprotonation.[21]

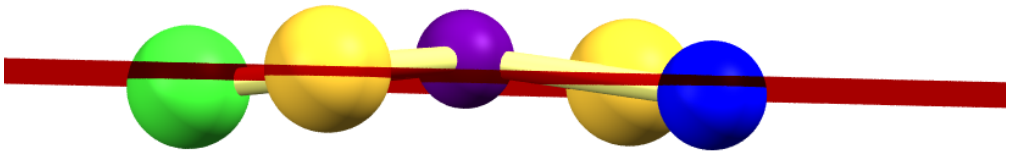

Figure 2.4: X-ray structure showing the base of the pyramid with respect to the copper out of the plane.

The absorption spectrum shown below contains a peak in the visible region at 620 nm with an extinction coefficient of 790 $M^{-1}cm^{-1}$ consistent with what is expected for a dark green solution (Figure 2.5). This peak can be assigned as a d-d transiton based on the small extinction coefficient. Another feature appears near the UV region at 390 nm (ε = 11 000 $M^{-1}cm^{-1}$) and is assigned a ligand-to-metal-charge transfer transition due to its large epsilon value.

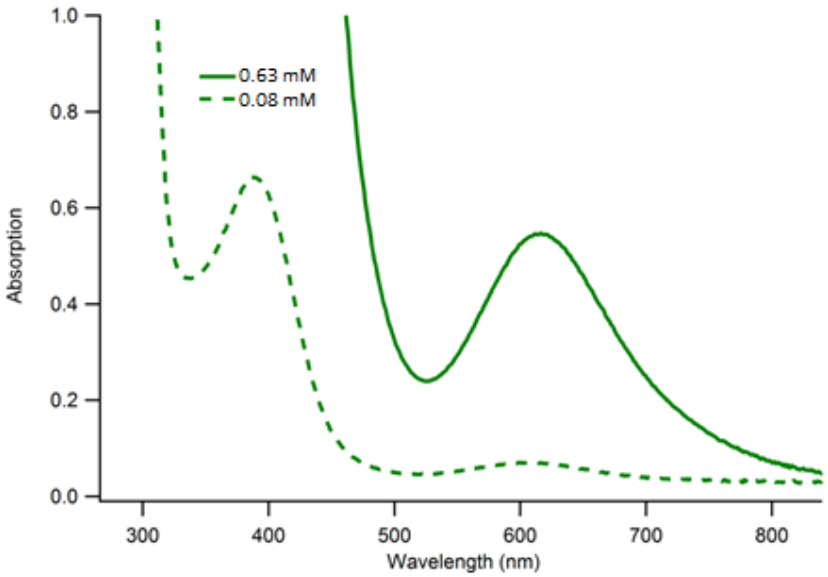

Figure 2.5: Absorption spectrum of $[Cu(SNSPhenyl)Cl]_2$

2.3.2 $[Cu(SNS_{t\text{-}butyl})X]_2$

Due to the insolubility of the complex $[Cu(SNS_{Phenyl})]_2^{2+}$ in solvents capable of supporting the desired acid/base chemistry, it was necessary to utilize a different R group. The previously synthesized $SNS_{t\text{-}butyl}$ pincer was used.[20] Initially, copper acetate monohydrate was used for metallation of the complex, which yielded an oil at room temperature. When placed in a freezer at -20° C, green needles precipitated and were analyzed by x-ray diffraction. The

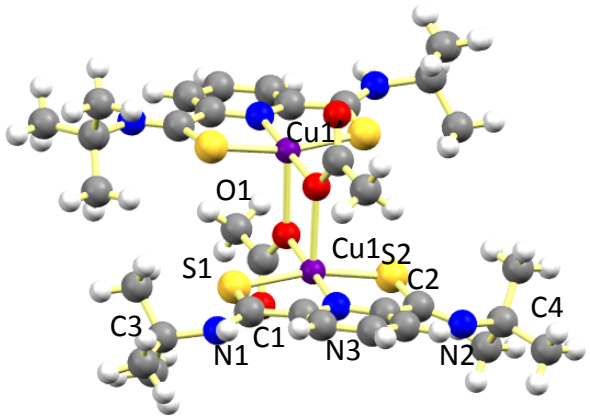

Figure 2.6: X-ray diffraction of $[Cu_2(SNS_{t\text{-}butyl})_2OAc_2]$

Table 2.2: $[Cu_2(SNS_{t\text{-}butyl})_2OAc_2]$

Selected Bond Lengths (Å)		Selected Bond Angles (deg)	
Cu1-S1	2.2894(13)	C1-N1-C3	126.9(4)
Cu1-S2	2.2349(13)	C2-N2-C4	123.7(4)
Cu1-O1	1.962(3)	Cu1-O1_Cu1'	101.39(12)
Cu1-N3	1.982(4)		
Cu1-O1'	2.402(3)		
S1-C1	1.679(5)		
C1-N1	1.322(6)		
C2-N2	1.276(6)		
S2-C2	1.755(4)		

structure indicates a mono-deprotonated ligand bound to the copper center (Figure 2.6). This ligand deprotonation state was seen in the SNS_{Phenyl} complex and in that instance a dimeric species formed in the solid state. There are similar bond distances in the C-S and C-N bonds compared to the $[Cu(SNS_{Phenyl})]^+$ thus justifying the mono-deprotonated assignment (Table 2.2). This structure differs from the complex described in section 2.2.1 in the distance between the copper centers and the bridging ligand, indicating the bridging oxygen is more symmetric with respect to the metal centers with bond distances of 2.25 Å and 2.40 Å to each copper center. This leads to a shorter Cu-Cu distance of 3.388 Å, which could lead to enhanced magnetic coupling. This change in the bridging ligand is most likely due to the bulky t-butyl groups compared to the phenyl groups the allow bridging through the sulfur. This complex is an oil at room temperature and is soluble in virtually all organic solvents. Due to the difficulties of working with an oil, synthesis using anhydrous copper chloride was explored.

Upon reaction of the $SNS_{t\text{-}butyl}$ ligand with anhydrous $[CuCl_2]$, a dark green solid precipitated out of acetonitrile. This product was filtered and recrystallized from DMF and ether. Crystals were obtained by ether diffusion into a concentrated solution of the complex in DMF. The structure shown below (Figure 2.7 and Table 2.3) is once again a bridged species, although the copper to apical chloride has a long bond distance of 2.7073(14) Å leading to the possibility that the species in solution is a monomer (only 82 % of the data set was collected). The steric hindrance of the t-butyl groups again prevents bridging through the thioamide

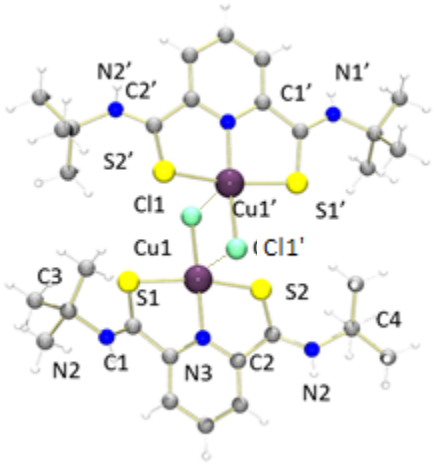

Figure 2.7: X-ray diffraction structure of $[Cu_2(SNS_{t\text{-}butyl})_2Cl_2]^{2+}$

Table 2.3: $[Cu_2(SNS_{t\text{-}butyl})_2Cl_2]$

Selected Bond Lengths (Å)		Selected Bond Angles (deg)	
Cu1-S1	2.2896(15)	C1-N1-C3	128.9(5)
Cu1-S2	2.2742(15)	C2-N2-C4	130.0(5)
Cu1-Cl1	2.2375(15)	Cu1-O1-Cu1'	86.46(5)
Cu1-N3	1.983(4)		
Cu1-Cl1'	2.7073(14)		
S1-C1	1.687(6)		
C1-N1	1.311(7)		
C2-N2	1.302(7)		
S2-C2	1.684(5)		

moiety. The Cu-Cu distance of 3.404 Å is only slightly longer than the acetate bridged species. The Cu center is slightly more out of the plane at the base of the pyramid at 0.137 Å toward the bridging chloride. Interestingly, the primary difference in the structure is that both of the hydrogens on the thioamide nitrogen appear to be present which requires the presence of a

counter anion for charge neutrality (omitted in Figure 2.7 for clarity). In fact there appears to be two counter ions; one a $CuCl_4$ and another $[CuCl_3(DMF)]$. The fact that the crystal structure indicates that the ligand is still doubly protonated allows for sequential base chemistry analogous to that performed by Kanbara and co-workers with a less expensive first row transition metal.

The initial reactions of complex $[Cu_2(SNS_{t\text{-}butyl})_2Cl_2]^{2+}$ titrated with triethylamine were performed in butyronitrile or dichloromethane (DCM) (non-coordinating or weakly coordinating solvents) due to the ability of these solvents to glass, which yielded unexpected results. The spectra obtained upon adding equivalents of triethylamine along with monitoring the absorption spectrum vs. number of equivalents in DCM indicates that the spectra continues to change even through the addition of 40 equivalents of triethylamine (Figure 2.8). This indicates that changes are observed not only upon deprotonation, but also with binding of triethylamine to the metal center. This seems plausible as triethylamine is not a good ligand so a large excess is required, although triethylamine bound is purely speculative.

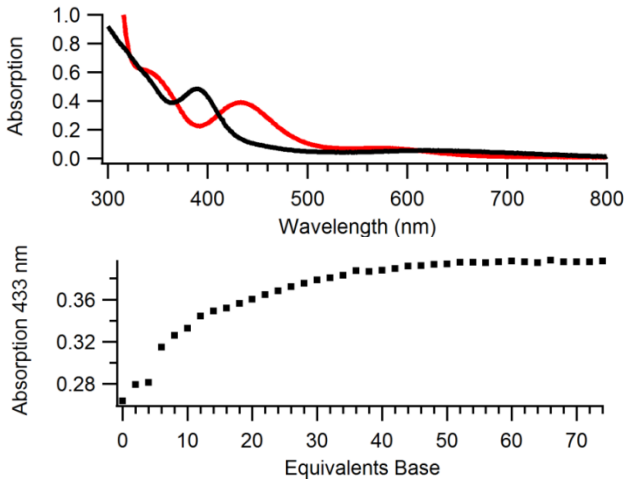

Figure 2.8: Top) Absorption spectrum $[Cu(SNS_{t\text{-}butyl})Cl]_2$ before addition of triethylamine (black) and after 74 equivalents of triethylamine (red). Bottom) Absorption at 433 nm versus equivalents of triethylamine added.

In contrast, when a coordinating solvent such as acetonitrile or DMF is used, the number of equivalents to induce complete change in the absorption spectrum decreases to two equivalents. The complete set of spectra clearly indicate that there are two separate events occurring upon addition of triethylamine, which could be either two separate deprotonation events or deprotonation followed by solvent binding to the metal center (Figure 2.9 and 2.10). It should also be noted that there are a series of isosbestic points in the absorption spectra from zero equivalents to 0.8 equivalents of triethylamine. These isosbestic points shift and remain from 0.8 equivalents and 1.8 equivalents of triethylamine further strengthening the notion that there are two separate events observed in the absorption spectra.

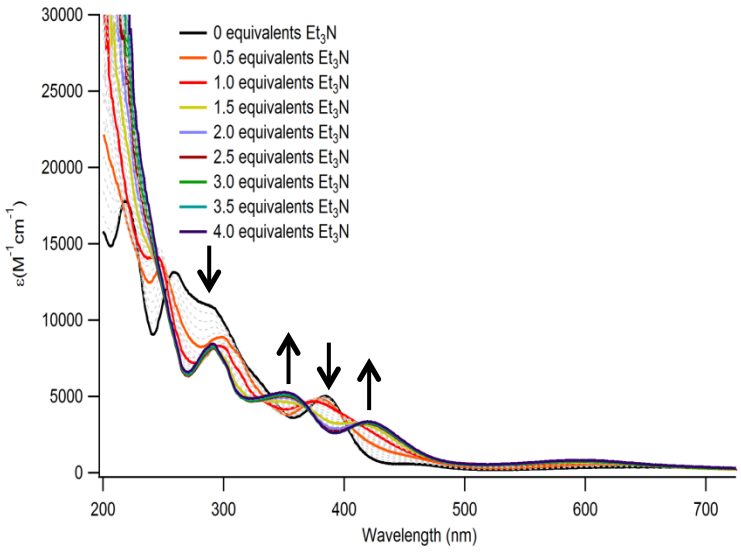

Figure 2.9: Absorption spectra of $[Cu^{II}(SNS_{t\text{-}butyl})Cl]_2^{2+}$ upon addition of triethylamine

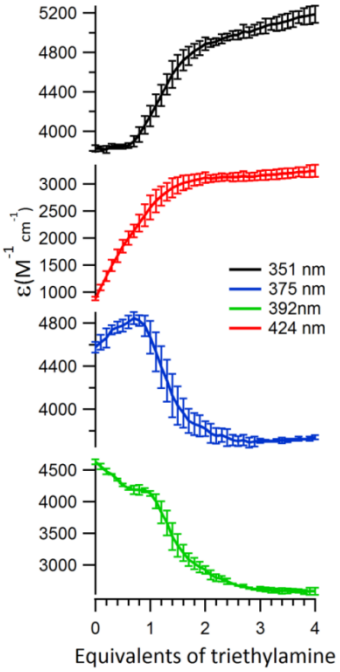

Figure 2.10: Titration curves of $[Cu^{II}(SNS_{t\text{-}butyl})Cl]_2$ upon addition of triethylamine

EPR data were also collected to corroborate the conclusion that after two equivalents of triethylamine a single new species is formed (Figure 2.11). This shows an initial rhombic system

with g_1= 2.17, g_2=2.05, and g_3=1.98. A four peak hyperfine coupling is observed in g_1 with a coupling constant of 171 G which results from the nuclear spin of 3/2 on copper. Based on the absorption spectra, samples were prepared with 0.7, 0.8, 2.0, and 4.0 equivalents of triethylamine. The samples prepared with 0.7 and 0.8 equivalents of triethylamine show significant signal broadening in the entire spectrum, but particularly noticeable is that the hyperfine peaks broaden dramatically indicating a mixture of species. At two equivalents, the spectrum becomes significantly more resolved but all of the features shifted to higher field with g_1= 2.12, g_2=2.03, and g_3=1.95 which is indicative of a different ligand field. The hyperfine coupling constant of 178 G also differs slightly. At four equivalents, there appeared to be no change from the sample with two equivalents. The sharpness of the final peaks as well as resolved hyperfine coupling on g_2 indicated that upon addition of two equivalents of triethylamine, there was a single new species.

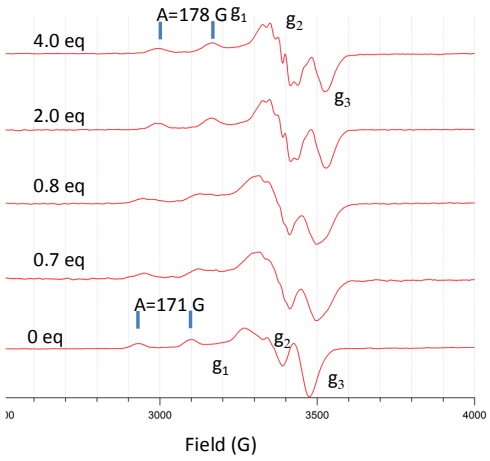

Figure 2.11: EPR spectra in acetonitrile of $[Cu(SNS_{t\text{-}butyl})Cl]_2$ with addition of triethylamine as labeled.

The same experiments were performed with DMF/DMA as the solvent system in order to get data from a glassy solvent and allow better resolution in EPR and perform MCD

experiments on the sample. An interesting result was obtained in the UV/vis experiments. The number of equivalents of triethylamine needed to break the first set of isosbestic point decrease to 0.4 equivalents. The number of equivalents of triethylamine required to observe what appear to be complete conversion of the starting species to the final species also decreases to 1.0 equivalent. This is believed to be due to the pH of the DMF:DMA solution being 9.3 and the pH of the acetonitrile solution being slightly acidic at 5.8 (based on values measured with a pH probe). The EPR data of the solution with DMF and DMA indicates that the complete change occurs at two equivalents of triethylamine (Figure 2.12).

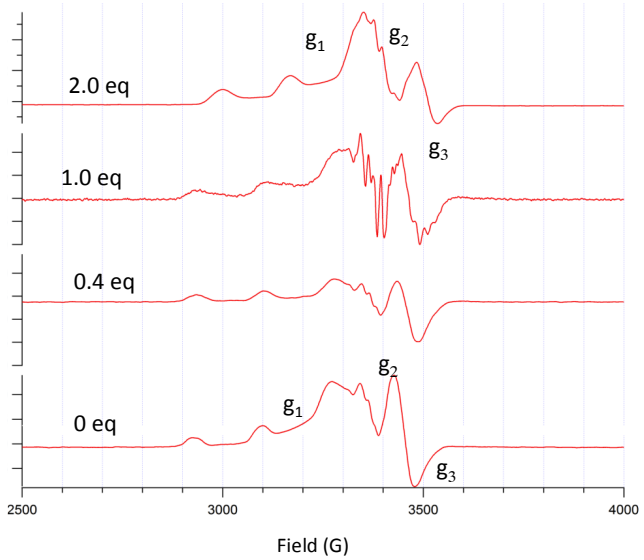

Figure 2.12: EPR spectra of $[Cu_2(SNS_{t\text{-}butyl})_2Cl_2]$ in 7:3 DMF:DMA with each addition of triethylamine labeled.

In an attempt to gain insight into what the new species at 2.0 equivalents of triethylamine is, crystals were grown by ether diffusion into a concentrated solution of complex in 7:3 DMF:DMA after addition of two equivalents of triethylamine. The structure of the complex indicates that there is no longer a dimer present and appears to be a mono-protonated thioamide complex with chloride as the fourth ligand (Figure 2.13 and Table 2.4).

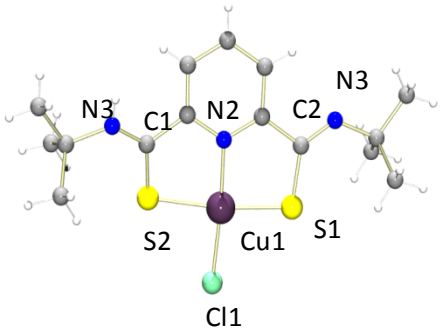

Figure 2.13: X-ray diffraction structure of Cu(SNS$_{t\text{-butyl}}$)Cl], formed after triethylamine was added to solution.

Table 2.4: Cu(SNS$_{t\text{-butyl}}$)Cl]

Selected Bond Lengths (Å)	
Cu1-S1	2.2966(10)
Cu1-S2	2.2323(11)
Cu1-Cl1	2.2477(11)
Cu1-N1	1.985(3)
S1-C2	1.693(3)
S2-C1	1.761(4)
C1-N2	1.316(5)
C2-N3	1.278(5)

These data are inconsistent with the data obtained in both UV/vis absorption and EPR. The fact that only one proton is taken by the triethylamine and the fourth ligand remains would be consistent with only a single event occurring upon titration with triethylamine. This leads to the conclusion that the solid state structure is not the same species that is in solution. To further prove this conclusion, absorption spectrum were taken before triethylamine was added and after triethylamine was added and then the product was crashed out of solution with ether. After crashing out, the solid was put back into solution and the spectrum taken again.

Figure 2.14 shows all of the spectra obtained. This indicates that the species that is crashed out of solution is neither the original species nor the species formed after two equivalents of base were added. Further studies need to be performed in order to understand the events that are occurring in solution.

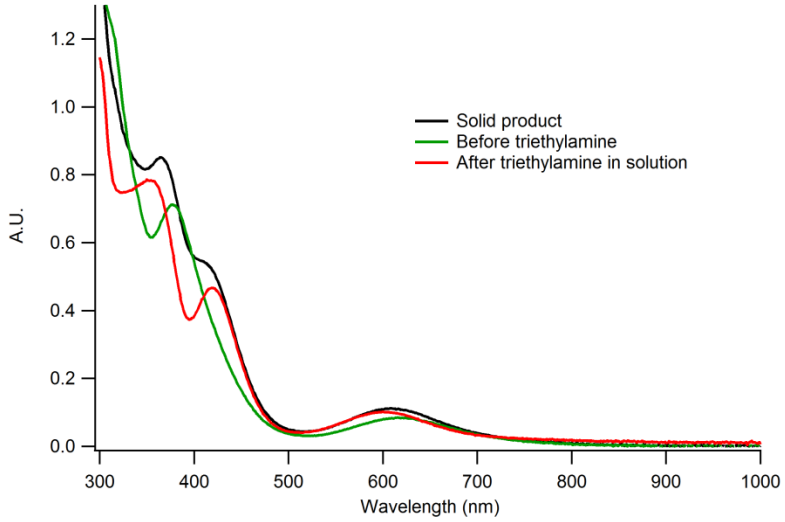

Figure 2.14: Absorption spectra of $[Cu^{II}(SNS_{t\text{-}butyl})Cl]^-$ (green); $[Cu^{II}(SNS_{t\text{-}butyl})Cl]^-$ and two equivalents of triethylamine; and $[Cu^{II}(SNS_{t\text{-}butyl})Cl]^-$ and two equivalents of triethylamine after being precipitated out.

2.4 Conclusion

A series of thioamide complexes were synthesized and characterized to understand their acid/base chemistry. UV-vis spectroscopy indicated that upon addition of triethylamine, two separate events occur. EPR spectroscopy also indicated that when 0.7 equivalents of triethylamine were added to the solution there was a mixture of species. Upon addition of a total of two equivalents of triethylamine a single new species was formed with a rhombic spectrum and g-values of g_1= 2.12, g_2=2.03, and g_3=1.95. While the nature of the two events

are unclear the likely possibilities are either two separate deprotonation events or a deprotonation followed by binding of solvent to replace the bound chloride ion. The solid state structure of the product after triethylamine addition indicates a different conclusion only indicating a single deprotonation event and no displacement of the chloride which would be consistent with a single event occurring upon addition of two equivalents of triethylamine. The fact that there is still one protonated thioamide and chloride remaining is believed to be an artifact of crystallization.

2.5 Future Experiments

The goal of this chapter was to explore acid/base chemistry of a thioamide copper complex. The ideal starting complex to study acid/base chemistry would be $[Cu(SNS_{t\text{-}butyl})Cl]_2$ as it begins in the doubly protonated state. The data collected to this point indicate that there are two separate events occurring in solution when triethylamine is added to the $[Cu(SNS_{t\text{-}butyl})Cl]_2$ complex, either two deprotonations or a deprotonation followed by acetonitrile (solvent) ligation. To explore whether the two events are indeed two separate deprotonations, cyclic voltammetry would be the ideal experiment to perform. This will lend insight into how many deprotonation events are occurring. If there are two deprotonation events occurring then two successive decreases in the Cu(II)/Cu(III) redox potential would be observed, one for each proton removed. There would also be a change in the redox potential if the chloride ligand were replaced by either DMF or acetonitrile. There would also be a change in the redox potential if solvent were bound to the copper ion. Finally, if the acid/base chemistry were to be explored in detail, the reverse reactions need to be explored as well. The same experimental

techniques (UV-vis, EPR, X-ray diffraction, and cyclic voltammetry) would be used in order examine whether upon addition of acid, the species returns to the original dithioamide Cu(II) complex.

References:

(1) Albrecht, M.; van, K. G. *Angew. Chem., Int. Ed.* **2001**, *40*, 3750.

(2) Cave, G. W. V.; Fanizzi, F. P.; Deeth, R. J.; Errington, W.; Rourke, J. P. *Organometallics* **2000**, *19*, 1355.

(3) Peris, E.; Loch, J. A.; Mata, J.; Crabtree, R. H. *Chemical Communications* **2001**, 201.

(4) Alsters, P. L.; Baesjou, P. J.; Janssen, M. D.; Kooijman, H.; Sichererroetman, A.; Spek, A. L.; Vankoten, G. *Organometallics* **1992**, *11*, 4124.

(5) Selander, N.; Szabo, K. J. *Chemical Reviews* **2011**, *111*, 2048.

(6) van der Vlugt, J. I. *European Journal of Inorganic Chemistry* **2012**, 363.

(7) Wang, Z. X.; Liu, N. *European Journal of Inorganic Chemistry* **2012**, 901.

(8) Balcells, D.; Clot, E.; Eisenstein, O. *Chemical Reviews* **2010**, *110*, 749.

(9) Milstein, D. *Topics in Catalysis* **2010**, *53*, 915.

(10) Leis, W.; Mayer, H. A.; Kaska, W. C. *Coordination Chemistry Reviews* **2008**, *252*, 1787.

(11) Vanderzeijden, A. A. H.; Vankoten, G. *Inorganic Chemistry* **1986**, *25*, 4723.

(12) Creaser, C. S.; Kaska, W. C. *Inorganica Chimica Acta* **1978**, *30*, L325.

(13) Begum, R. A.; Powell, D.; Bowman-James, K. *Inorg. Chem.* **2006**, *45*, 964.

(14) Hossain, M. A.; Lucarini, S.; Powell, D.; Bowman-James, K. *Inorg. Chem.* **2004**, *43*, 7275.

(15) Koizumi, T.-a.; Teratani, T.; Okamoto, K.; Yamamoto, T.; Shimoi, Y.; Kanbara, T. *Inorg. Chim. Acta* **2010**, *363*, 2474.

(16) Okamoto, K.; Kuwabara, J.; Kanbara, T. *J. Organomet. Chem.* **2011**, *696*, 1305.

(17) Teratani, T.; Koizumi, T.-a.; Yamamoto, T.; Kanbara, T. *Inorg. Chem. Commun.* **2011**, *14*, 836.

(18) Teratani, T.; Koizumi, T.-a.; Yamamoto, T.; Tanaka, K.; Kanbara, T. *Dalton Trans.* **2011**, *40*, 8879.

(19) Teratani, T.; Koizumi, T.-a.; Yamamoto, T.; Tanaka, K.; Kanbara, T. *Dalton Trans* **2011**, *40*, 8879.

(20) Wang, Q.-Q.; Ara, B. R.; Day, V. W.; Bowman-James, K. *Inorg. Chem. (Washington, DC, U. S.)* **2012**, *51*, 760.

(21) Kapoor, R.; Kataria, A.; Kapoor, P.; Pannu, A. P. S.; Hundal, M. S.; Corbella, M. *Polyhedron* **2007**, *26*, 5131.

Structural and Spectroscopic Characterization of Cu(I) and Cu(II) Amide Complexes and Reactivity with Potassium Superoxide

Chapter 3

3.1 Introduction

3.1.1 Copper Enzymes

Copper cofactors in biology perform a diverse array of functions from oxidation to electron transfer. The active site of many metalloproteins have been studied in great detail, however, the proposed active intermediates are typically studied using small molecule mimics due to the reduced complexity that these systems offer. In regards to copper containing enzymes, Cu(I) is typically the oxidation state of the resting cofactor allowing the metal center to readily oxidize to Cu(II) and Cu(III) for functional purposes. In some extracellular proteins, such as prion protein (PrP,) which was discussed in the introduction, Cu(II) is shown to bind with much greater affinity then Cu(I), however a number of other divalent metals have been shown to bind with similar affinity in vitro.[1-3] The explanation for this finding is a result of the ligand field stabilization that Cu(II) is able to achieve due to the geometry about the metal center. Cu(I) is a d^{10} metal which is unstable in square planar geometry due to the $d_{x^2-y^2}$ being doubly occupied at much higher energy, thus making it unlikely to bind. This (PHGGGWGQ) octarepeat region contains amino acid residues 60-91 in which the metal binding site is either the four histidine residues (His 61, 69, 77, 85) in the case of low copper concentration, or the histidine (His 61), glycine (Gly 62), glycine (Gly 63), glycine (Gly 64) residues in the case of high copper concentration.[4] This change in coordination allows for a much lower Cu(II)/Cu(III) redox potential. This lowering of the redox potential is proposed to allow for interaction with superoxide in vivo.[5-11]

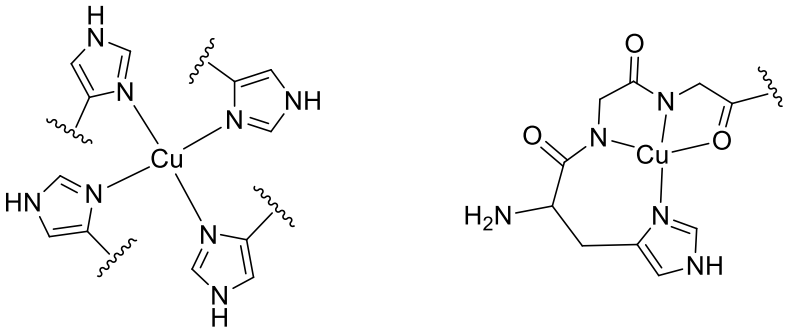

Figure 3.1: Copper binding in PrP left: µM concentration of copper. Right: nM concentration of copper.

3.1.2 KO_2 reactivity with Cu(II) complex

Due to the debate over the function of PrP, small molecule mimics that interact with superoxide are necessary to show precedence for the proposed function. Cu(I) is known to react with oxygen, superoxide, or peroxide to form a number of coordination types.[12] The oxygen can bind to either one metal center in an end-on fashion or side-on fashion and, depending on the redox potential of the metal center, can be a superoxo or peroxo (Scheme 3.1). When a second metal is involved the binding modes can get even more complicated.[12] In a recent communication, Tolman and co-workers, reported the binding of a superoxide anion to a Cu(II) metal center utilizing an amide pincer ligand which supports a similar square planar geometry as that found in PrP.[13] The reported complex was characterized by electronic absorption spectroscopy and X-ray absorption spectroscopy and compared to computations. What makes this finding interesting is the manner in which the complex was formed. Typically molecular oxygen is the oxidant used in copper oxygen chemistry, which when forming a bridging peroxo complex oxidizes both centers by one electron. In this case, superoxide was

bound in such a manner as not to oxidize the metal center. The formation was further confirmed when a Cu(I) complex known to form and end-on peroxo complex was put in solution with the superoxide complex and the absorption spectrum showed the characteristic feature of a Cu(II:II) *trans*-μ-1,2-peroxo species being formed, formally oxidizing Cu(I) to Cu(II).[14] This species has been shown to form an intense band at 624 nm (ε=8300 $M^{-1}cm^{-1}$). While this work itself is very interesting, little work was done where two copper ions are in a similar geometry in close proximity with each other, as is the case with prion protein. For the current study superoxide anion was added to the Cu(II) macrocycle (Figure 3.2) yielding an interesting change in the absorption spectrum showing two peaks grow in intensity but the features decay rapidly at room temperature.

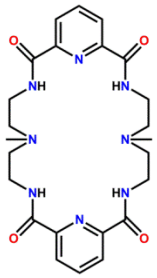

Figure 3.2: PyEtAm Ligand

Scheme 3.1: Copper oxygen species from reaction of oxygen with Cu(I) as initial oxidation state

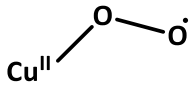

End-on superoxo

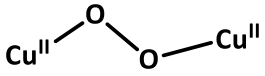

End-on peroxo (trans-μ-1,2-peroxo)

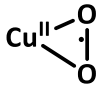

Side-on superoxo

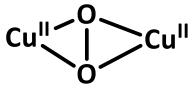

Side-on peroxo (μ-$\eta^2\eta^2$-1,2-peroxo)

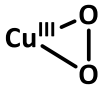

Side-on peroxo

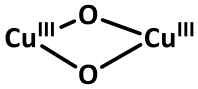

Bis(μ-oxo)

3.2 Ligands and complexes Discussed in this Chapter

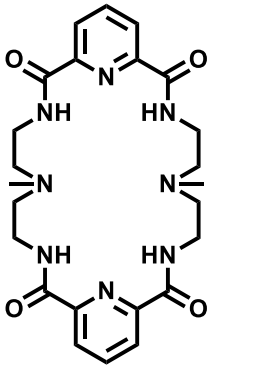

PyEtAm Macrocycle

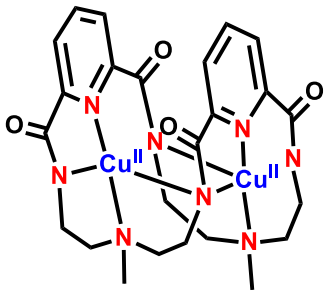

$[Cu_2(PyEtAm_{H-4})]$

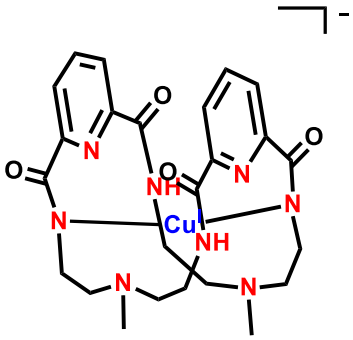

$[Cu_2(PyEtAm_{H-2})]^-$

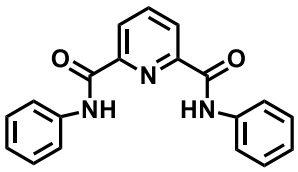

NNN_{Phenyl}

3.3 Results and Discussion

3.3.1 $[Cu(PyEtAm_{H-2})]^+$

Copper(I) is a diamagnetic d^{10} ion which allows for solution characterization of Cu(I) complexes via NMR. The PyEtAm macrocyclic ligand used for complexation was previously synthesized in the Bowman-James lab and is shown Figure 3.2.[15] The Cu(I) complex with the PyEtAm macrocycle indicates a that upon metal binding the macrocycle is only doubly deprotonated in the solid state structure leaving a negative charge on the complex (Figure 3.3 and Table 3.1). This structure shows a single copper center bound in the center of the macrocycle. The Cu(I) is two coordinate with a nearly linear geometry having a bond angle of 173.32(10)° between the two amide nitrogens. The Cu-N_{amide} bond distance is relatively short at 1.880(2) Å and 1.882(2) Å. The metal center has weak interactions with the pyridine rings with a distance of 2.62Å. The counter cation is the sodium ion, and it holds the two macrocycles together through an interaction with the amide oxygens. The absorption spectrum of the $[Cu(PyEtAm_{H-2})]^-$ is also shown below and is a relatively featureless spectrum with an intense charge transfer band at high energy (Figure 3.4). This is to be expected for a d^{10} metal which is void of any *d-d* transitions.

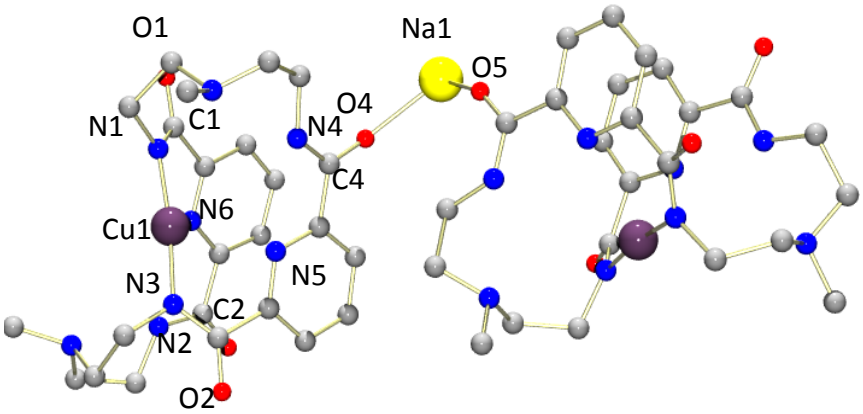

Figure 3.3: X-ray diffraction structure of $[Cu(PyEtAm_{H-2})]^-$

Table 3. 1: $[Cu2PyEtAm_{H-2}]^-$

Bond Lengths (Å)	
Cu1-N1	1.880(2)
Cu1-N2	1.882(2)
N1-C1	1.322(3)
N2-C2	1.325(3)
N3-C3	1.322(4)
N4-C4	1.321(3)
C1-O1	1.266(3)
C2-O2	1.239(3)
C3-O3	1.256(3)
C4-O4	1.236(3)
O4-Na1	2.270(2)
O5-Na1	2.288(2)

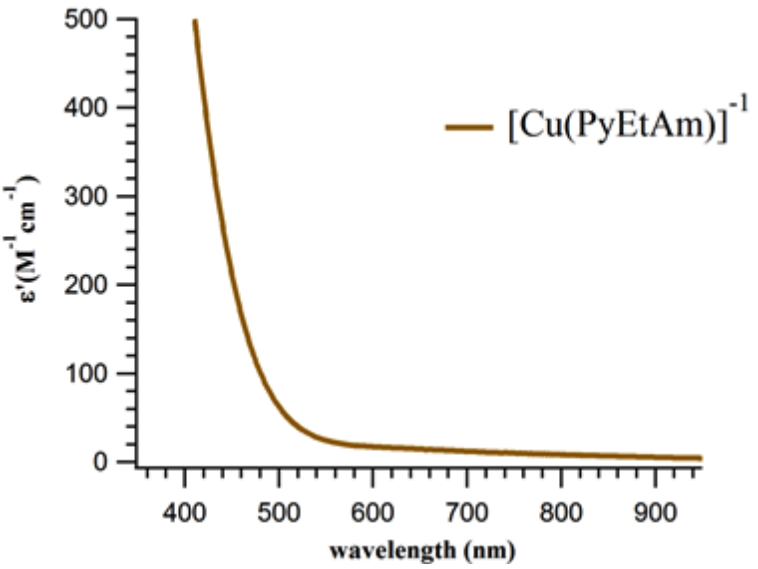

Figure 3.4: Absorption spectrum of $[Cu(PyEtAm_{H-2})]^-$

3.3.2 $[Cu_2(PyEtAm_{H-4})]$

The Cu(II) macrocycle complex was previously synthesized and characterized and is shown in section 3.2.[15] The m/z $(ESI)^+$ is known to be 620.1 and the absorption spectrum shows an asymmetric broad feature at 590 nm (ε = 310 $M^{-1}cm^{-1}$). However, the work in this chapter aims to further characterize the complex using magnetic circular dichroism spectroscopy (MCD) and electron paramagnetic resonance spectroscopy (EPR) in order to gain insight into the electronic ground state of the complex. From the MCD spectra, we see that the absorption peak is actually comprised of at least two separate transitions at 560 nm and 670 nm (Figure 3.5). Upon deconvolution of the spectrum, the visible region is shown to have four d-d

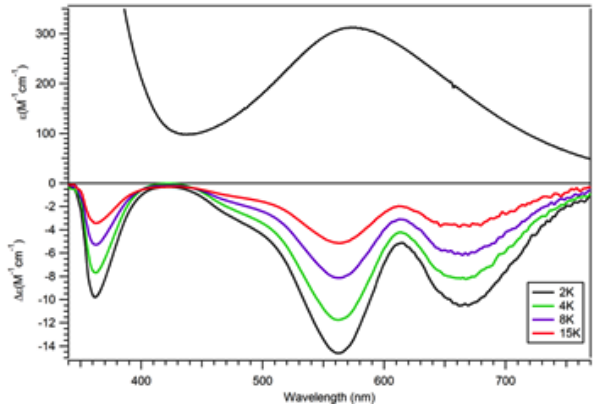

Figure 3.5: Absorption (top) and MCD (bottom) spectra of [Cu_2(PyEtAm$_{H-4}$)]

transitions. These transitions are to be expected from a square planar d^9 complex. Variable-temperature,variable-field (VTVH) MCD spectroscopy performed allowed for the spin-state of the [Cu_2(PyEtAm$_{H-4}$)] complex to be determined. The isotherms obtained do not overlay which is consistent with an S_{tot} > 1/2 system (Figure 3.6). To further probe the ground state of the complex, EPR data was obtained at 5 K (Figure 3.7). This data indicate a rhombic system with g_1 = 2.67, g_2 = 2.24, and g_3 = 1.86 which is typical of an S=1/2. Upon closer examination a signal at g=4.18 is also present and is assigned to the forbidden $\Delta M_s = \pm 2$ transition. The highly resolved

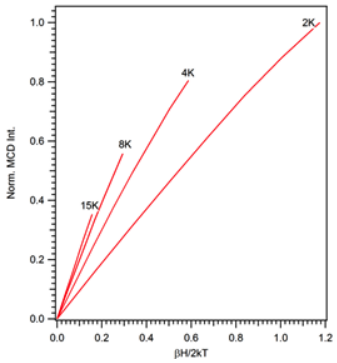

Figure 3.6: VTVH MCD data of [Cu_2(PyEtAm$_{H-4}$)]

Figure 3.7: EPR spectrum of [Cu_2(PyEtAm$_{H-4}$)]

nature of this spectrum shows seven hyperfine peaks from the coupling of the two Cu(II) centers. These data are indicative of a complex with an integer spin state. Together with the VTVH data, the conclusion can be made that the ground state is a ferromagnetically coupled system in which the two S = ½ copper ions align to give the complex an overall spin of *S* = 1.

The spectroscopic data allows for the exploration of the electronic ground state of a Cu(II) amide complex. Amide ligation is a vital part of bioinorganic chemistry as every protein backbone contains the amide moiety. The ligation in this case is very similar to the manner in which Cu(II) is bound in PrP in a high copper concentration environment as both are bound to two amide nitrogens and an imine nitrogen.[4,7,9,10,16] The fourth coordination site for the protein is an oxygen and for this complex it is an amine.

3.3.3 $[Cu_2(PyEtAm_{H-4})] + KO_2$

Based on the work out of the Tolman Lab showing a Cu(II) complex interacting with superoxide, similar work was done using the Cu(II) macrocycle complex.[13,15] A solution of KO_2 and 18-crown-6 ether was mixed with a solution of $[Cu_2(PyEtAm_{H-4})]$ at low temperatures.[17] The initial spectrum consists of just KO_2 and is featureless in the visible region. Upon addition of $[Cu_2(PyEtAm)]$, the spectrum changes to the red spectrum and has intense features in the high energy visible region (Figure 3.8). These transitions are presumably ligand-to-metal-charge transfer as *d-d* transitions are not likely to have such large extinction coefficients. For clarity, the spectrum of the initial $[Cu_2(PyEtAm_{H-4})]$ has also been included and the extinction coefficient for this visible transition (~310 $M^{-1}cm^{-1}$) is much more likely to be a *d-d* transition. It is important to note that upon disappearance of the charge transfer band, the spectrum does not revert back to the $[Cu_2(PyEtAm_{H-4})]$, but instead the visible peak has shifted to slightly higher energy. As seen in the previous section, the solid state structure of the $[Cu_2(PyEtAm_{H-4})]$ complex indicate a square pyramidal complex (shown as the dinuclear species in Figure 3.9).

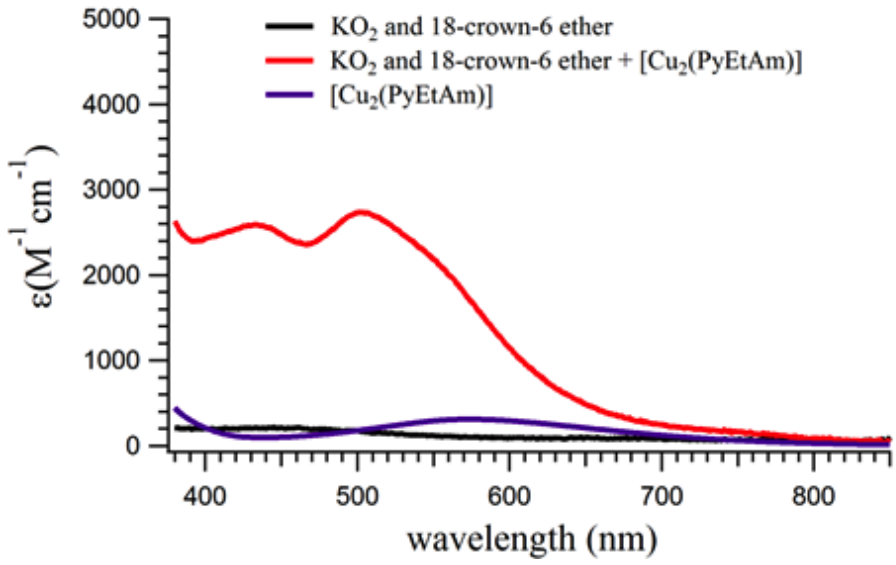

Figure 3.8: Absorption spectra of $[Cu_2(PyEtAm)]$ (purple); Slurry of KO_2 and 18-crown-6-ether (black); and a mixture of $[Cu_2(PyEtAm)]$ and KO_2 and 18-crown-6-ether all in DMF at -50° C (red).

3.3.4 $[Cu(PyEtAm_{H-2})]^+ + O_2$ contamination

When the same procedure to synthesize $[Cu(PyEtAm_{H-2})]^+$ is followed with a slight contamination of molecular oxygen, a green solution is obtained. Upon evaporation of solvent and recrystallization via ether diffusion into methanol two different crystals were obtained: green and yellow plates. The yellow plates were consistent with the $[Cu(PyEtAm_{H-2})]^+$ while the green plates, alternatively, had not been previously identified. The green plates were also characterized via XRD and the structure is shown in Figure 3.9. The unit cell is comprised of two ligands and three copper centers along with a cationic Na. The complex is a combination of $[Cu(PyEtAm_{H-2})]^+$ and $[Cu_2(PyEtAm_{H-4})]$ which are bridged through the Na^+. The Cu-ligand distances are very similar to those seen in the individual crystals of the $[Cu(PyEtAm_{H-2})]^+$ and $[Cu_2(PyEtAm_{H-4})]$ species. The geometry about the sodium cation is distorted tetrahedral with

slightly shorter bond distances than in the $[Cu(PyEtAm_{H-2})]^+$, with the protonated amide oxygen bond distance being the longest at 2.27Å. A different synthetic method was used to obtain $[Cu_2(PyEtAm_{H-4})]$, in the absence of base, Na^+ was absent in the crystal lattice. It is speculated that the formation of the co-crystallized species occurs because of slight O_2 contamination present in NaH dispersed in mineral oil.

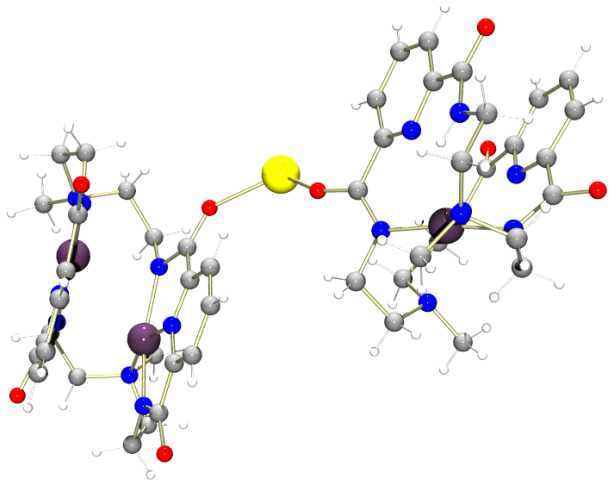

Figure 3.9: Co-crystallized $[Cu_2(PyEtAm_{H-2})]^-$ and $[Cu_2(PyEtAm_{H-4})]$ bridged through a sodium ion (yellow).

Absorption data of $[Cu_2(PyEtAm_{H-2})]^+$ and $[Cu_2(PyEtAm_{H-4})]$ were obtained and compared to the co-crystallized system. $[Cu_2(PyEtAm_{H-4})]$ has a d-d transition typical of a d^9 complex at ~585 nm with an extinction coefficient of 311 ($M^{-1}cm^{-1}$), as well as an intense charge transfer transition in the UV region. $[Cu_2(PyEtAm_{H-2})]^+$, being a d^{10} complex void of any *d-d* transitions, shows only a strong absorption band in the UV region of the spectrum, beginning at slightly lower energy than $[Cu_2(PyEtAm_{H-4})]$. The spectrum of the co-crystallized complex shows that

there are two independent complexes in solution as it reveals an additive spectrum of $[Cu_2(PyEtAm_{H-2})]^+$ and $[Cu_2(PyEtAm_{H-4})]$. It has a *d-d* transition at 585 nm with an extinction coefficient of 320 ($M^{-1}cm^{-1}$) (figure 3.10 top). The charge transfer band beginning at lower energy is also observed.

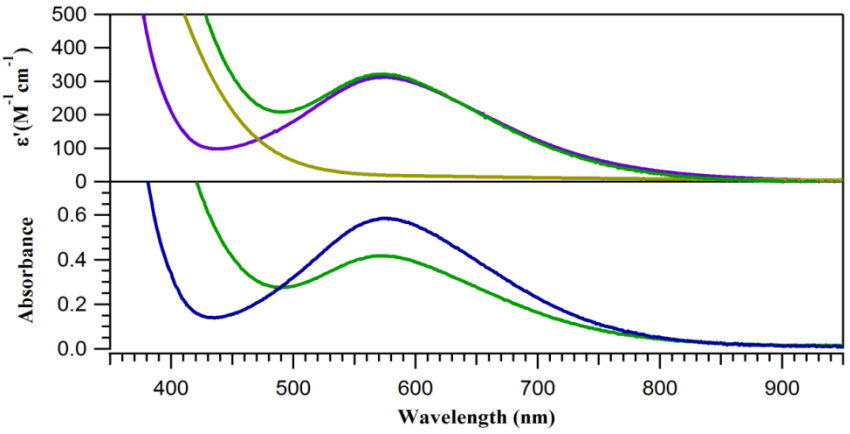

Figure 3.10: Top) Absorption spectrum of $[Cu^{II}_2(PyEtAm_{H-4})]$ (purple); $[Cu^{I}(PyEtAm_{H-2})]^-$ and $[Cu^{II}_2(PyEtAm_{H-4})]$ (green); and $[Cu^{I}(PyEtAm_{H-2})]^-$ (golden). Bottom) $[Cu^{I}(PyEtAm_{H-2})]^-$ and $[Cu^{II}_2(PyEtAm_{H-4})]$ before exposure to oxygen (green) ; and $[Cu^{I}(PyEtAm_{H-2})]^-$ and $[Cu^{II}_2(PyEtAm_{H-4})]$ after exposure to oxygen (purple).

To investigate the possibility that oxygen causes $[Cu_2(PyEtAm_{H-2})]^-$ to convert to $[Cu_2(PyEtAm_{H-4})]$, the co-crystallized complex was exposed to O_2 for 48h to allow the reaction to go to completion, and the new absorption spectrum was recorded (Figure 3.10 bottom). Upon exposure to O_2 the band at 585nm grew in intensity and the charge transfer band shifted to higher energy. When comparing the absorption of the mixed co-crystallized complex at 585 nm to the extinction coefficient of $[Cu_2(PyEtAm_{H-4})]$ a concentration of 1.25 mM was calculated. Once the sample was oxidized, the band at 585 nm was calculated to have a concentration of

1.76 mM. This would indicate that the Cu(I) species was able to be oxidized with molecular oxygen.

Copper mixed valent species are not a rare occurrence in the literature. Typically these systems are indicative of two types, Type II and Type III. [18-22] These systems differ only in the location of the unpaired electron. In Type II, the unpaired electron is localized about a single Cu(II) center. In contrast, Type III has an unpaired electron that is delocalized about the two metal centers. This work indicates that in the solid state this is a Type II system as the unpaired electron is localized. The oxygen reactivity of the complex in solution seems to indicate that this is not the structure in solution, but merely a consequence of crystallization. This is not surprising as the sodium cation and the copper complexes likely dissociate upon solvation. If the structure remained in solution, the rigidity would likely prevent two anionic complexes to come into close enough proximity to allow for oxidation to occur in a manner that would allow for formation of a [Cu($PyEtAm_{H-4}$)] and giving a free ligand.

3.3.5 $[Cu_2(NNN_{Phenyl})]^{2-}$

To further explore the Cu(I) chemistry with this backbone that typically binds first row transition metal in a square planar or square pyramidal geometry we utilized a pincer ligand that prefers to bind metals in a three coordinate, equatorial manner. In 2000, Mukherjee and co-workers synthesized a hydroxo bridged Cu(II) complex utilizing N,N'-diphenyl-2,6-pyridinedicarboxamide (NNN_{Phenyl}) as a ligand (Figure 3.11).[23] This ligand has been utilized in

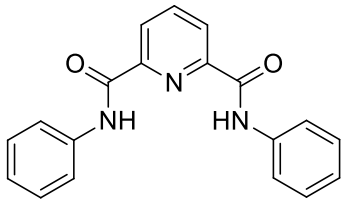

Figure 3.11: NNN_{Phenyl} Ligand

interactions with a variety of metals including nickel, iron, and cobalt. The iron and cobalt complexes have shown the ability to interact with molecular oxygen affording oxidation of the metal center from M^{2+} to M^{3+}. It was because of this capability that Cu(I) appeared to be an exciting pathway to explore. Initially, like the work with the macrocycle, the ligand binds in an equatorial manner like other pincers with solvent or a fourth anionic ligand bound. This is not the a typical geometry found in Cu(I) complexes as is outlined in the introduction. The reaction of $[Cu(CH_3CN)_4]OTf$ with the NNN_{Phenyl} ligand in DMF with base resulted in the formation of a dark red solution. Following a number of recrystallizations and an ether diffusion into a concentrated solution of DMF, dark red crystals were obtained for analysis by X-ray diffraction. The structure shows that there are two Cu(I) ions and two ligands which form a helical structure around the metal centers (Figure 3.12). The crystal structure shows the pyridines not symmetrically bound between the metal centers (Table 3.2). The NMR shows this to be an artifact of the crystal packing. In the NMR there are five signals to be seen with integrations similar to what would be expected if the complex binds in a symmetrical fashion. The peak assignments can be made and are shown in Table 3.3 based on the labeling scheme shown in the top of Figure 3.13. The pyridine peaks are further downfield compared to the phenyl rings,

which is similar to the free ligand. All of the peaks are shifted downfield when compared with the free ligand as is seen in Figure 3.13 (bottom).

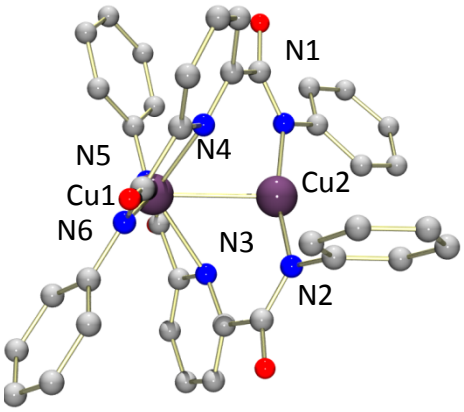

Figure 3.12: X-ray diffraction structure of $[Cu_2(NNN_{Phenyl})]^{2-}$

Table 3.2: $[Cu_2(NNN_{Phenyl})]^{2-}$

Bond Lengths (Å)		Bond Angles (deg)	
Cu1-Cu2	2.7107(11)	N1-Cu1-N2	156.3
Cu1-N5	1.955(4)	N1-Cu1-N4	104.0
Cu1-N6	1.938(4)	N3-Cu1-N4	118
Cu1-N3	2.202(4)	N3-Cu2_N4	101
Cu1-N4	2.295(4)	N5-Cu2-N6	164.49
Cu2-N1	1.906(4)		
Cu2-N2	1.923(4)		

Table 3. 3: Assignment based on lettering scheme in Figure 3.12

Proton	^{1}H Shift Complex	^{1}H Shift Ligand
A	N/A	11.05(2H,*s*)
B	7.97(2H,*d*)	8.41(2H,*d*)
C	7.87(1H,*t*)	8.32(1H,*t*)
D	7.19(4H,*d*)	7.924H,*d*)
E	6.81(4H,*t*)	7.46(4H,*t*)
F	6.59(2H,*t*)	7.21(2H,*t*)

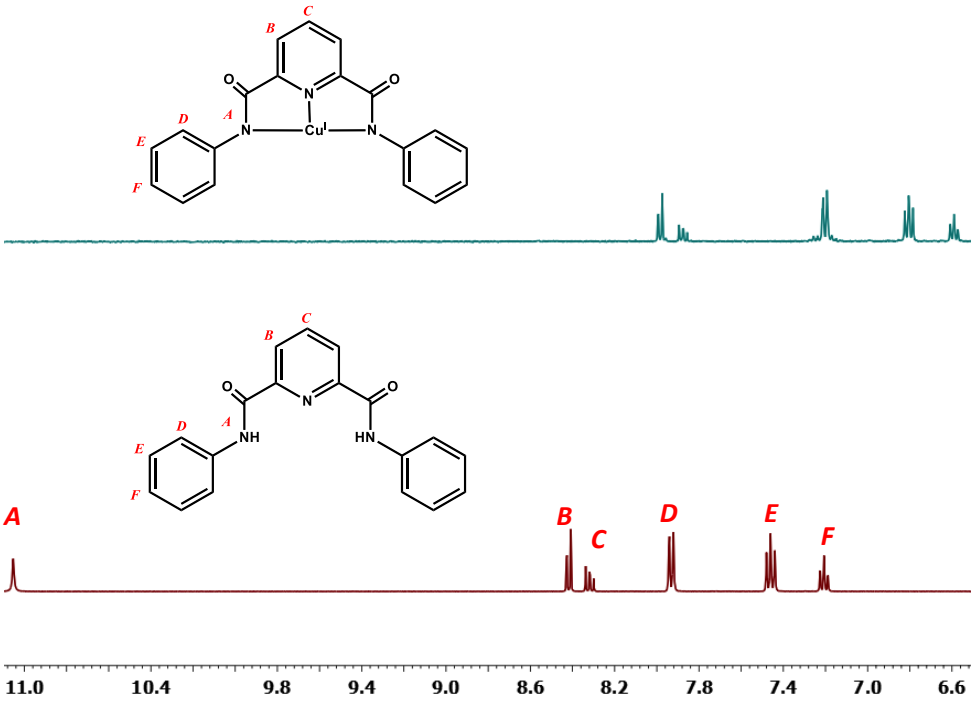

Figure 3.13: ^{1}H NMR spectra of $[Cu_2(NNN_{Phenyl})_2]^{2-}$ (top) and NNN_{Phenyl} bottom.

3.4 Conclusion

In this chapter it was shown that the tetramido/diamine macrocycle was able to form a complex with a Cu(I) cation. This complex was shown to be reactive toward molecular oxygen to form the known Cu(II) macrocycle while liberating a free ligand. The Cu(I) complex, as is seen from the crystal structure, has the ability to bind in nearly linear fashion to a macrocycle which had been shown to bind transition metals in either a square planar, square pyramidal, or octahedral geometry. This ability was also shown with the pincer backbone in the case of the amide acycle. The Cu(II) complex was shown to have ferromagnetic electronic coupling between the unpaired electrons of the Cu(II) centers. This was evident by both VTVH MCD data and EPR spectroscopy. The Cu(II) complex was also shown to be reactive with superoxide to form an unstable intermediate. This intermediate appears to have a significant metal to ligand charge transfer as the extinction coefficients in the absorption spectrum are far too large to be $d \rightarrow d$ transitions.

3.5 Future Experiments

The goal of this chapter was to characterize both Cu(I) and Cu(II) complexes with amide ligands. The Cu(II) macrocyclic complex has been characterized utilizing a multitude of spectroscopic methods. The most exciting portion of this chapter in terms of novel work is that involving the reaction of the Cu(II) macrocycle with superoxide. The species that is formed upon addition of potassium superoxide to the $[Cu_2(PyEtAm_{H-4})]$ is still largely uncharacterized. The first experiment that needs to be performed is resonance Raman spectroscopy as this is the benchmark method for characterizing metal-oxygen species. The O-O stretch will allow for

determination of the oxidation state of the O_2 ligand, whether superoxo or peroxo. If the product is a peroxo, then the O-O stretch would appear between 740 and 830 cm^{-1} depending on the manner in which the peroxo binds.[12] If the product were a superoxo, the O-O stretch would appear at higher energy between 960 and 1150 cm^{-1}.[12] And if the product happened to be a bis-μ-oxo, the core breathing mode appears at ~600 cm^{-1}.[12] While resonance Raman will clearly indicate what the metal oxygen species is, EPR spectroscopy should be used to determine the oxidation state of the copper center(s) in this species. If the species contains an end-on superoxo copper(II) unit, then the unpaired spins of the Cu(II) and superoxo will likely pair antiferromagnetically, yielding a diamagnetic system that is EPR-silent. In support, the previously reported [Cu^{II}(N,N'-bis(2,6-diisopropylphenyl)-2,6-pyridinecarboxamide)($O_2^{\bullet -}$)] complex formed by Tolman and co-workers was found to have an S = 0 ground state.[13] A peroxo-bridged dicopper(II,II) would also be expected to be EPR-silent due to antiferromagnetic coupling of the two Cu(II) centers, but resonance Raman would distinguish this species from a mononuclear superoxo Cu(II) species. Alternatively, a peroxo-bridged dicopper (II,III) species whould be expected to be EPR active (S = $^1/_2$). If the species is EPR-silent, ^{1}H NMR could be attempted to characterize the bound ligand. The last method that would be useful is copper K-edge x-ray absorption spectroscopy (XAS). This would provide complementary information regarding the metal oxidation state as the edge energy in an x-ray absorption experiment is a direct indication of the oxidation state of the metals center as is shifts to higher energy with increasing oxidation state. XAS experiments also have the potential to provide insight into the coordination sphere of the metal center through analysis of extended x-ray absorption fine structure (EXAFS) data.

References:

(1) Millhauser, G. L. *Ann. Rev. Phys. Chem.* **2007**, *58*, 299.

(2) McMahon, H. E. M.; Mange, A.; Nishida, N.; Creminon, C.; Casanova, D.; Lehmann, S. *J. Biol. Chem.* **2001**, *276*, 2286.

(3) Yamamoto, N.; Kuwata, K. *Chem. Phys. Lett.* **2010**, *498*, 184.

(4) Davies, P.; Brown, D. R. *Biochemical Journal* **2008**, *410*, 237.

(5) Brown, D. R. *Folia Neuropathologica* **2005**, *43*, 229.

(6) Brown, D. R.; Kozlowski, H. *Dalton Transactions* **2004**, 1907.

(7) Chattopadhyay, M.; Walter, E. D.; Newell, D. J.; Jackson, P. J.; Aronoff-Spencer, E.; Peisach, J.; Gerfen, G. J.; Bennett, B.; Antholine, W. E.; Millhauser, G. L. *Journal of the American Chemical Society* **2005**, *127*, 12647.

(8) Davies, P.; Marken, F.; Salter, S.; Brown, D. R. *Biochemistry* **2009**, *48*, 2610.

(9) Hodak, M.; Bernholc, J. *Prion* **2010**, *4*, 13.

(10) Liu, L.; Jiang, D. L.; McDonald, A.; Hao, Y. Q.; Millhauser, G. L.; Zhou, F. M. *Journal of the American Chemical Society* **2011**, *133*, 12229.

(11) Millhauser, G. L. In *Annual Review of Physical Chemistry* 2007; Vol. 58, p 299.

(12) Mirica, L. M.; Ottenwaelder, X.; Stack, T. D. P. *Chemical Reviews* **2004**, *104*, 1013.

(13) Donoghue, P. J.; Gupta, A. K.; Boyce, D. W.; Cramer, C. J.; Tolman, W. B. *Journal of the American Chemical Society* **2010**, *132*, 15869.

(14) Paul, P. P.; Tyeklar, Z.; Jacobson, R. R.; Karlin, K. D. *Journal of the American Chemical Society* **1991**, *113*, 5322.

(15) Ghosh, S.; Roehm, B.; Begum, R. A.; Kut, J.; Hossain, M. A.; Day, V. W.; Bowman-James, K. *Inorganic Chemistry* **2007**, *46*, 9519.

(16) Millhauser, G. L. *Accounts of Chemical Research* **2004**, *37*, 79.

(17) Donoghue, P.; Gupta, A.; Boyce, D.; Cramer, C.; Tolman, W. *Journal of the American Chemical Society* **2010**, *132*, 15869.

(18) Dunajjurco, M.; Ondrejovic, G.; Melnik, M.; Garaj, J. *Coordination Chemistry Reviews* **1988**, *83*, 1.

(19) Gupta, R.; Zhang, Z. H.; Powell, D.; Hendrich, M. P.; Borovik, A. S. *Inorganic Chemistry* **2002**, *41*, 5100.

(20) LeCloux, D. D.; Davydov, R.; Lippard, S. J. *Journal of the American Chemical Society* **1998**, *120*, 6810.

(21) Westmoreland, T. D.; Wilcox, D. E.; Baldwin, M. J.; Mims, W. B.; Solomon, E. I. *Journal of the American Chemical Society* **1989**, *111*, 6106.

(22) Williams, K. R.; Gamelin, D. R.; LaCroix, L. B.; Houser, R. P.; Tolman, W. B.; Mulder, T. C.; deVries, S.; Hedman, B.; Hodgson, K. O.; Solomon, E. I. *Journal of the American Chemical Society* **1997**, *119*, 613.

(23) Patra, A. K.; Ray, M.; Mukherjee, R. *Polyhedron* **2000**, *19*, 1423.

Synthesis and Characterization of a Para-xylyl Cobalt Cryptand Complex and the Role of Water in its Reactivity with CO_2

Chapter 4

4.1 Introduction

Cryptands have been utilized in chemistry for a variety of uses such as small molecule activation or fixation with metal cryptands and anion binding. [1-6] Work with cryptand ligands began in the late 1960's with alkaline and alkali earth metals and in the early 1970's grew to include transition metal complexe (Figure 4.1).[7-11] The work with transition metals began in order to study bimetallic systems with the metal centers at an adequate distance to allow the exploration of bridging substrates. These complexes were coined cascade or inclusion complexes and began to involve bridging anions. This work, pioneered by Jean-Marie Lehn, looked to explore the use of bridging imidazole ligands thought to be relevant in biological inorganic chemistry.[8,12-14] The scope of this chapter involves the use of cryptands in transition metal binding.

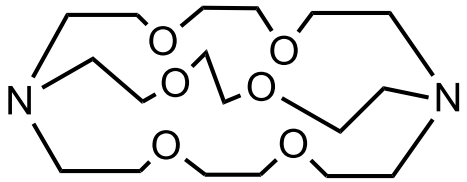

Figure 4.1: Early cryptand synthesized by Lehn and co-workers.[15]

Transition metal binding was first explored using tris(2-aminoethyl)amine (TREN) based macrobicycles. The nitrogen atoms are able to form bonds with the transition metals and form dinuclear species, which the previously studied polyether linked cryptands lacked.[5,6] A large number of linking groups have been utilized to form these complexes allowing for the metal-metal distance to be tuned for specificity in molecular recognition.[11-14,16] Using transition metal complexes led researchers to utilize absorption spectroscopy to analyze the binding of a given

anion. This is due to the *d-d* transitions of the transition metal complex often occurring in the visible region. The fact that a given ion will affect the ligand field environment in a manner that allows the transition to differ in energy and be quantified through simple absorption spectroscopy is very useful.[5] In addition to changing optical properties of these complexes, perturbations in magnetic properties were also explored. The coupling of the unpaired spins were able to change based on the binding mode of the anion. In 1992, Harding and co-workers explored a series of metal cryptand complexes and investigated how their electron coupling was affected by anion interactions using the cryptands.[5] These researchers found that in the case of Cu(II) cryptand complexes with bridging anions such as hydroxide that there was a small antiferromagnetic coupling, which is in contrast to previously reported Cu(II) cryptand complexes with an azide bridge that showed large antiferromagnetic coupling.[5,17,18] These complexes have also shown practical use beyond simple anion binding into the realm of CO_2 fixation.[3]

4.1.2 Dinucear Cryptand Complexes and Small Sequestration

CO_2 sequestration has been studied and characterized in a number of systems.[19-21] Sequestration of CO_2 is useful in many processes including solar energy storage[22,23] and as a source of carbon-containing compounds.[20,21] Recently, Lu and co-workers synthesized a dinuclear Cu(II) cryptate complex that has the ability to transform carbon dioxide to the carbonate monoester form of the alcoholic solvent in which the reaction took place.[3] The reaction with the alcohol is proposed to proceed through the mechanism shown below (Scheme 4.1). The product of the reaction is an example of how CO_2 sequestration could form a

source of useful carbon containing compounds. Even more interesting is that this reaction is able to proceed forward even in slightly acidic conditions. These reactions typically occur in basic media as this would help to form the hydroxide precursor necessary for sequestration of the CO_2 through nucleophilic attack on the electrophilic carbon. This reaction is made possible due to the proximity of one metal center to the other, allowing a concerted reaction to take place. The proximity of the metal centers has other implications, including the formation of radical coupling to form oxygen-oxygen bonds.

Scheme 4.1: *m*-xylyl connector omitted for clarity

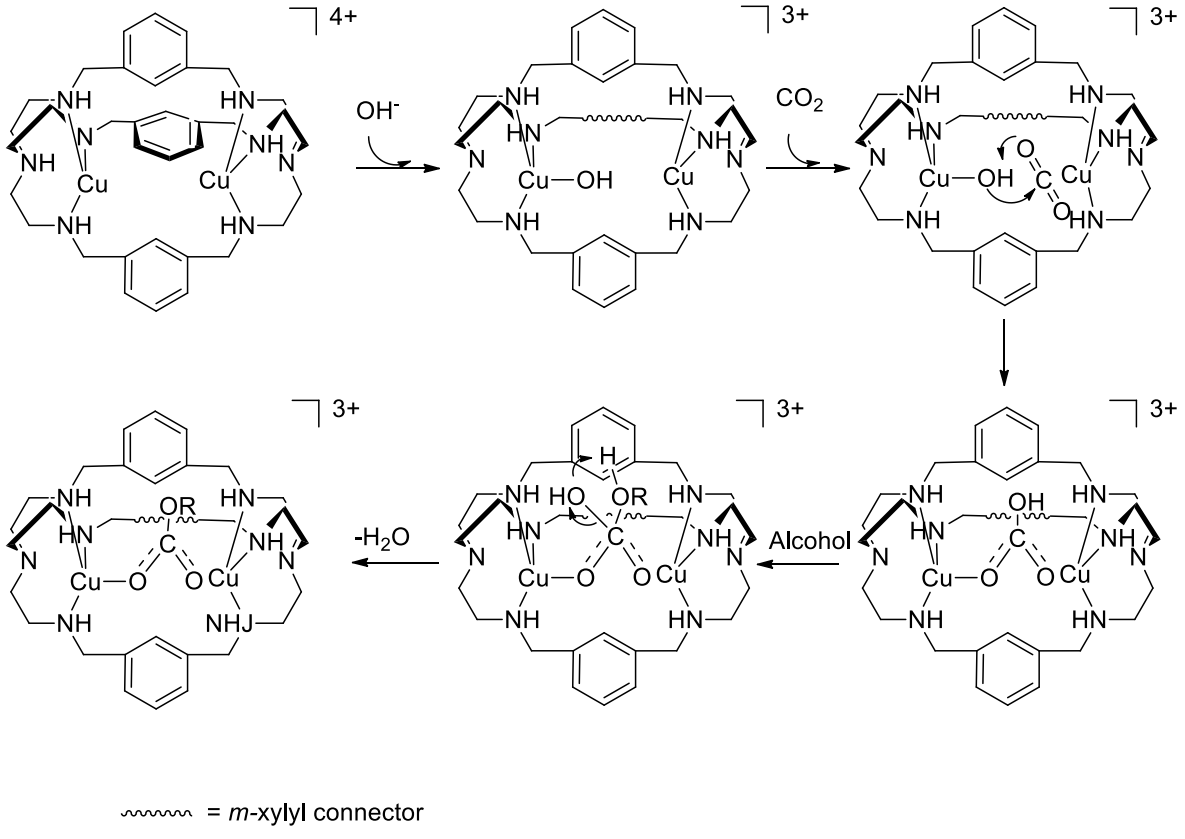

In 2008, Nocera and co-workers reported an amide based cryptand complex based on a ligand synthesized in the Bowman-James lab (Figure 4.2).[24-27] The goal of this work was to utilize the hexaanionic nature of the ligand to support high valent metal-oxo species for oxygen-oxygen bond formation through a radical mechanism. As mentioned previously, the proximity of the metal centers allows bridging substrates. The goal of this work was to bring two reactive oxygen species together with the goal of allowing them to react and form molecular oxygen. The metal centers were shown to be capable of moving in the cavity in the presence of a bridging ligand which was thought to allow enough flexibility for such a reaction to take place. In 2010, and subsequently in 2011, there was a family of complexes with first row transition metals that were synthesized and characterized.[25,26] Although the goal of this research was never achieved, a number of absorption spectra were obtained showing the ability to bind cyanide between two metal centers. These species were also shown to couple in a weakly antiferromagnetic fashion. Noteworthy is the fact that in 2012 this same group was able to show, in the free ligand, the ability to disproportionate potassium superoxide into peroxide and molecular oxygen as was seen by an x-ray crystal structure showing peroxide bound in the cavity.[1]

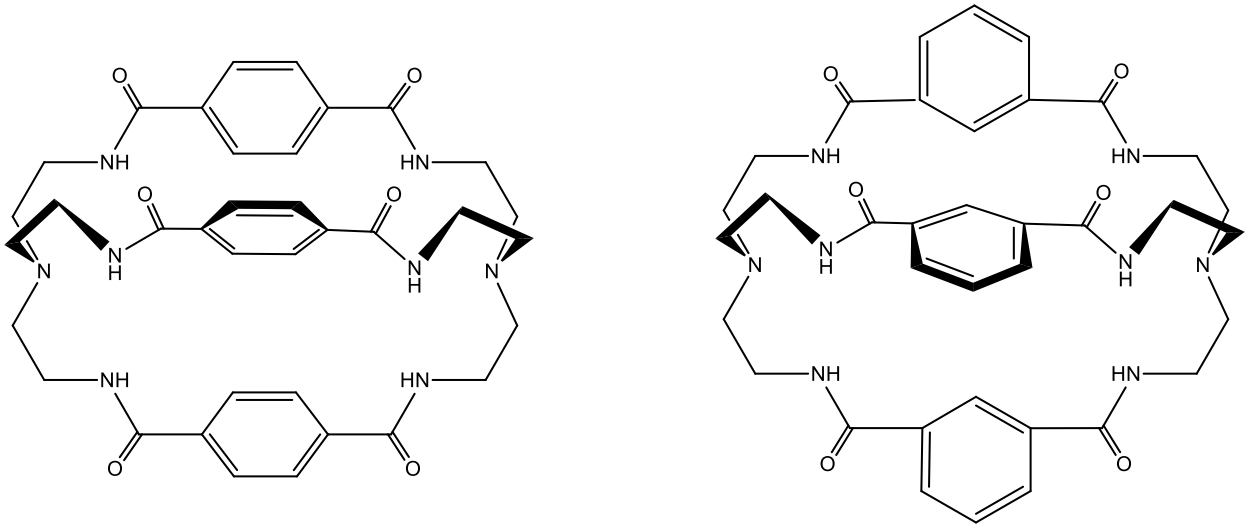

Figure 4.2: Cryptand ligands synthesized by the Bowman-James group (Nocera's version is a meta-xylyl version with bulky alkanes in the 4 position for enhanced solubility).

4.2 Ligands and Complexes Discussed in this Chapter

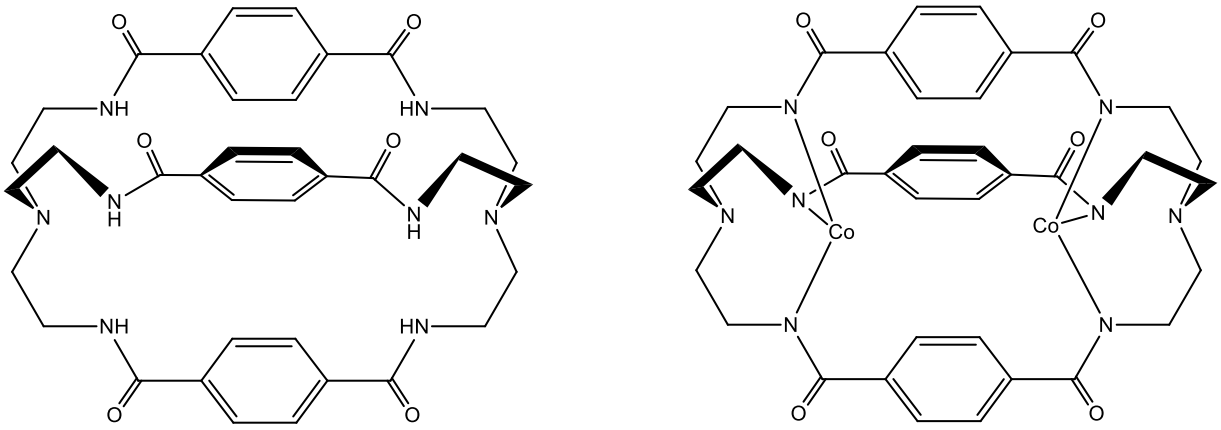

Cryptand $[Co_2(Cryptand_{H-6})]^{2-}$

4.3 Results and Discussion

4.3.1 $[Co_2(cryptand_{H\text{-}6})]^{2-}$

Using a very similar metallation to that mentioned in the literature, a Co(II) cryptand was synthesized (63.44 % yield).[25] The absorption spectrum of the product (Figure 4.3) appears very similar to the spectrum of the cobalt *m*-xylyl cryptand obtained by Nocera and co-workers and is typical of a Co(II) spectrum. There is a *d-d* transition at 580 nm with an extinction coefficient of 140 (M^{-1} cm^{-1}) and another feature just slightly higher in energy. The MCD spectrum contains a *d-d* transition at 610 nm and 590 nm (Figure 4.4). The VTVH data shows that the isotherms of the indicated bands do not overlap, although the data were never fitted to allow for assignment of spin state (Figure 4.5). An ^1H NMR spectrum was obtained, but was found not to be useful as there was significant signal broadening due to the paramagnetic cobalt centers. Crystals suitable for x-ray diffraction were obtained by methanol evaporation of the complex (Figure 4.6 and Table 4.1). The structure confirmed what mass spectrometry indicated, a fully deprotonated ligand bound to two metal centers positioned within the TREN moiety The unit cell consists of two cryptand complexes bridged through the amide oxygens to a potassium. This motif has been seen previously with the bridging sodium in the case of the co-crystallized species from chapter three. The cobalt sits 0.228 Å out of the plane of the three equatorial amide nitrogens raised away from the bridgehead nitrogen. The Co-Co distance is long at 6.793 Å although the previously reported cryptand structures were shown to be flexible and bind anions between the two metal centers. Based on these reports these complexes appeared to be suitable for CO_2 binding.

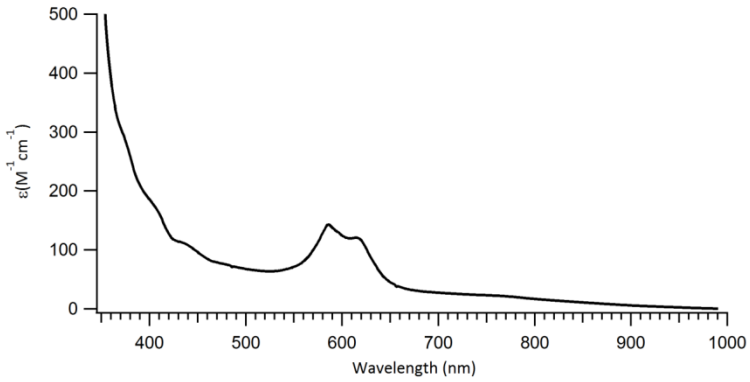

Figure 4.3: Absorption spectrum of $[Co_2(cryptand_{H\text{-}6})]^{2-}$

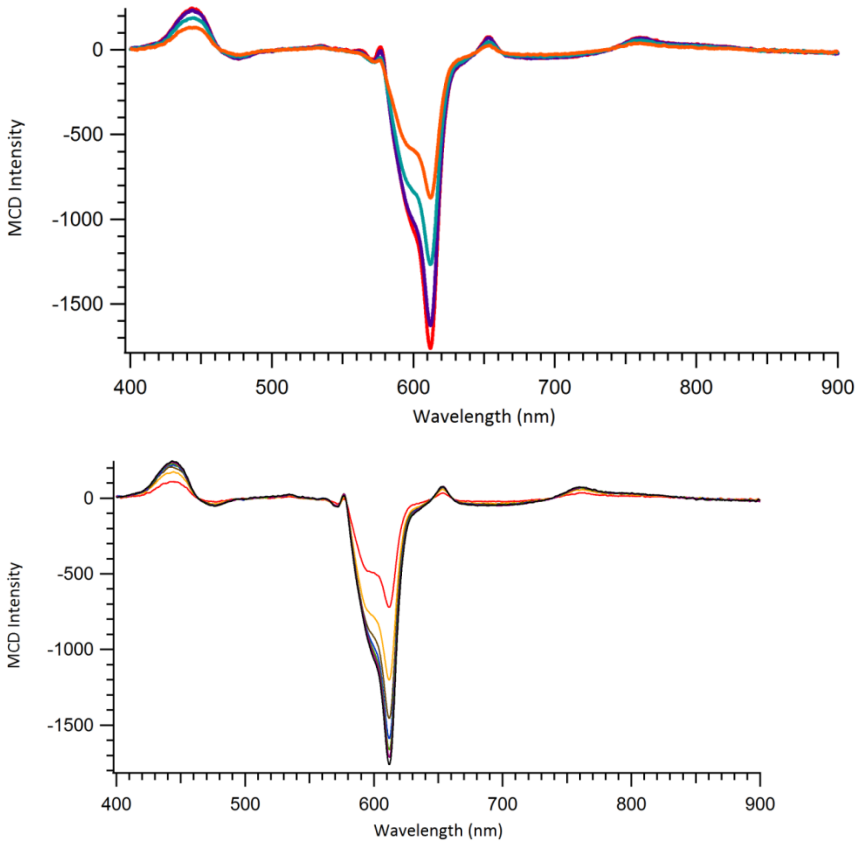

Figure 4.4: Top) MCD data collected at 7T at 2K (red), 4K (violet), 8K (teal), and 15K (orange). Bottom) MCD data collected at 2K and 7T (black), 6T (violet), 5T (green), 4T (blue), 3T (brown), 2T (orange), and 1T (red).

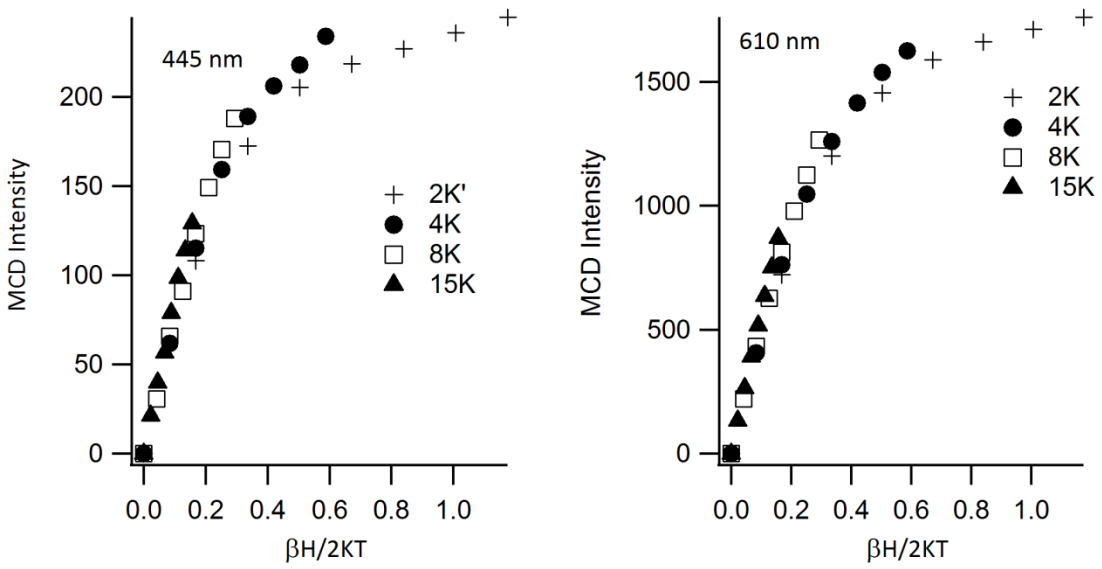

Figure 4.5: VTVH data collected at 445 nm (left) and 610 nm (right).

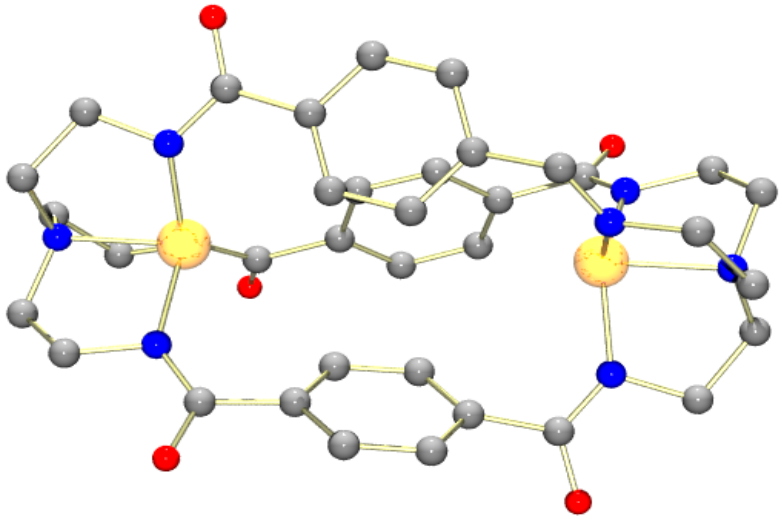

Figure 4.6: X-ray diffraction structure of $[Co_2(cryptand_{H\text{-}6})]^{2-}$ with hydrogens and potassiums omitted for clarity.

Table 4.1: $[Co_2(cryptand_{H\text{-}6})]^{2-}$

Bond Lengths (Å)	
Co-$N_{bridgehead}$ (avg)	2.094
Co-N_{amide} (avg)	1.985
Co-Co	6.793

4.3.2 $[Co_2(cryptand_{H\text{-}6})]^{2-} + CO_2$

Reactivity with CO_2 was performed by observing changes in the absorption spectrum after bubbling CO_2 through a solution of the cobalt complex in DMF. The baseline begins to increase indicating light scattering from the formation of a precipitate. An attempt to characterize the precipitate was performed by first collecting the precipitate by filtration through a fine frit. After collection of the precipitate, the solid was placed into DMSO and stirred vigorously. The solid was found to be insoluble in DMSO as well as any other organic or aqueous solvents. The literature indicated that cobalt carbonate was a mineral that was insoluble in anything except organic acids, and the only way to characterize it was by infrared spectroscopy (IR) or powder x-ray diffraction.[28] A sample of the precipitate was made into a KBr pellet, and the IR spectrum was obtained (Figure 4.7). The IR spectrum was compared to a sample published in 2009 from Zeng and co-workers.[29] The published article indicates that the primary feature is an intense band at 1477 wavenumbers (cm^{-1}). The published spectrum shows that the feature appears to be at a high concentration and the feature absorbs 100 % of the light between 1477 and 1600 cm^{-1}. The feature present in the spectrum obtained in this work has a band at approximately the same energy which is consistent with the C-O stretch of the cobalt carbonate. The published spectrum also has weaker signals at 864 cm^{-1} and 744 cm^{-1}. The spectrum obtained herein has low signal to noise ratio and does not allow the lower energy bands to be resolved. Another spectrum in the Spectral Database for Organic Compounds SDBS was obtained as a nujol mull. A second IR experiment was performed as a

nujol mull for the precipitate in this section. The published spectrum in nujol shows a peak at 1464 cm^{-1} and a second feature at 1378 cm^{-1} similar to the spectrum in KBr. The experimentally obtained spectrum in nujol has features at similar energy (Figure 4.8). A weaker transition for the published spectrum in nujol was at 732 cm^{-1}. While this feature is not obtained experimentally, a band at 720 cm^{-1} is present. While the IR evidence suggests the formation of cobalt carbonate, these data are by no means conclusive and the future experiments sections discusses ways to possibly further validate this conclusion. A second question to investigate was how the precipitate was forming.

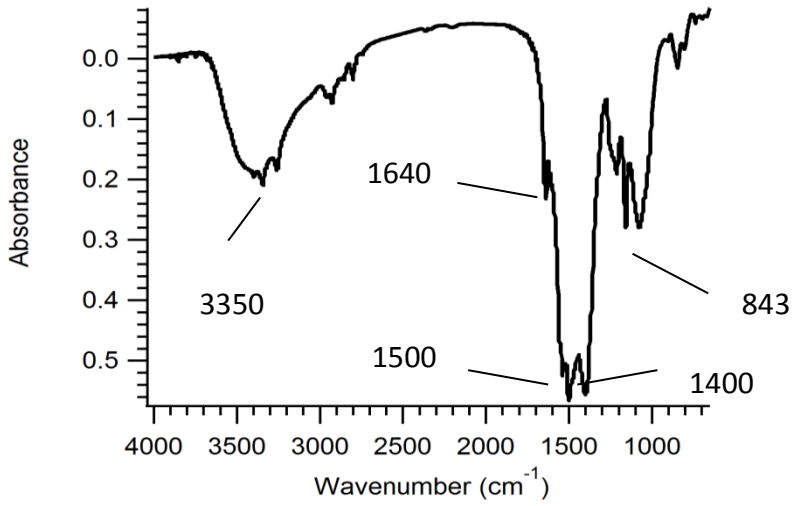

Figure 4.7: KBr pellet IR spectrum, precipitate from bubbling CO_2 through cobalt cryptand solution

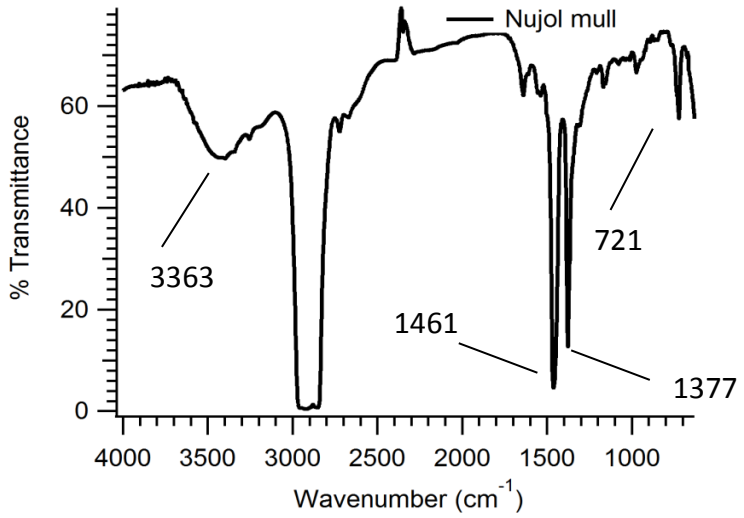

Figure 4.8: Nujol mull IR spectrum, precipitate from bubbling CO_2 through cobalt cryptand solution

To address this question, conditions were altered upon bubbling of CO_2. The first variable altered was the amount of water that was in the sample. This was changed due to the equilibrium of water and CO_2 converting to bicarbonate and a proton (Scheme 4.2). In order to study the effect of water, two separate vessels are used to dissolve the cobalt complex, one with DMSO that was spiked with water and the other in anhydrous DMSO (Sigma-Aldrich) and stored in a glove box. The CO_2 was ran through a drying tube prior to bubbling through the solution. The absorption spectra of both samples were collected and the peaks at 587 nm and 617 nm were observed with respect to time. The anhydrous sample was seen to have a linear decay in the peaks at 587 nm and 617 nm still present after 1300 min, although their intensities had decreased (Figure 4.9). In contrast, the water spiked sample undergoes almost complete decay after only 300 min (Figure 4.10). The anhydrous sample decreased linearly with time, while the water spiked sample decreases exponentially (Figure 4.11). This data thus indicate that water is required for the reaction to proceed. It is proposed that the decrease in

absorption for the anhydrous sample was cause by humidity from the atmosphere slowly leaching into the sample through the rubber septa.

Scheme 4.2:

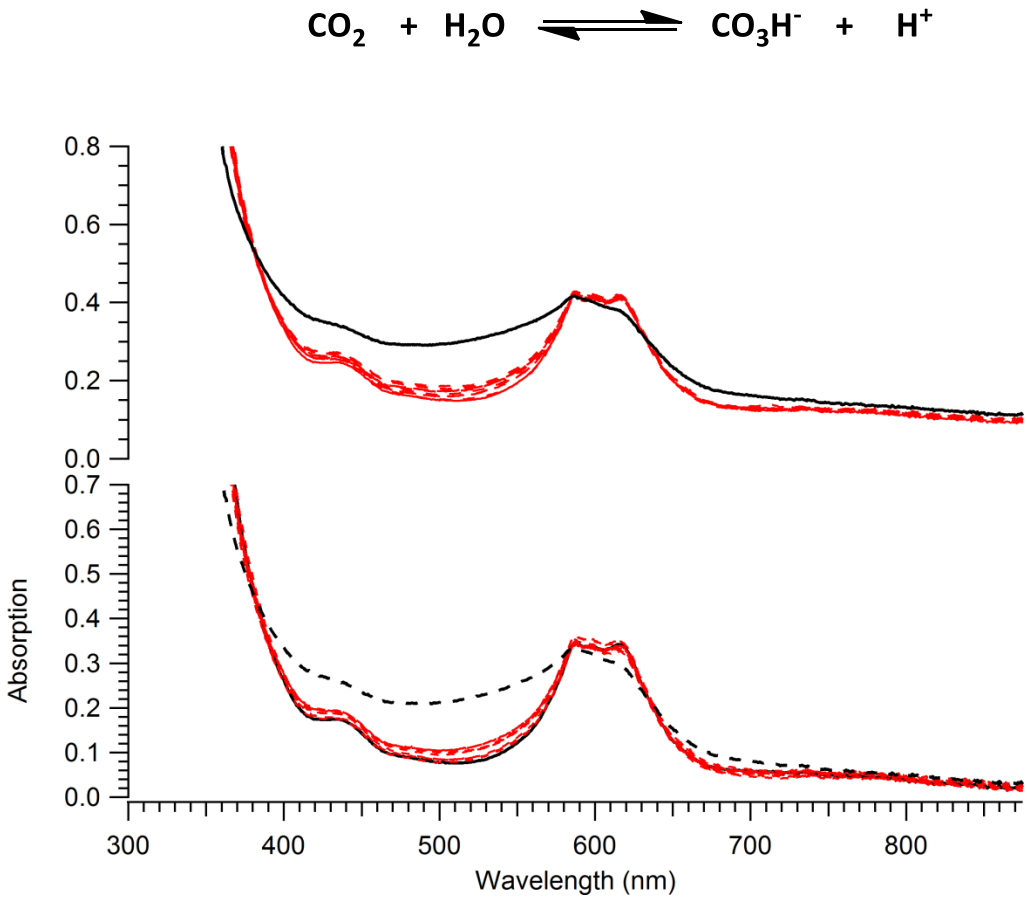

Figure 4.9: Uncorrected UV-vis absorption data from anhydrous DMSO (top). UV-vis absorption data with baseline correction at 1000 nm in anhydrous DMSO (bottom). Immediately after bubbling (black solid), and 14.75 h after bubbling (black dashed). Red traces are representative of the plots taken over time.

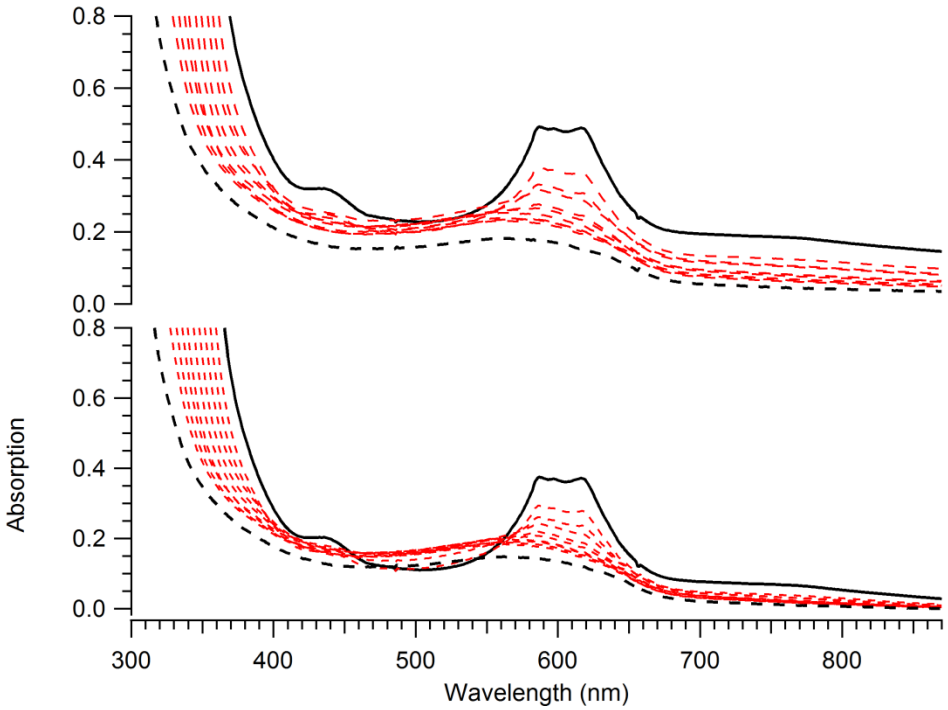

Figure 4.10: Uncorrected UV-vis absorption data in water spiked DMSO (top). UV-vis absorption data with baseline correction at 1000 nm in water spiked DMSO (bottom) Immediately after bubbling (black solid), and 14.75 h after bubbling (black dashed).

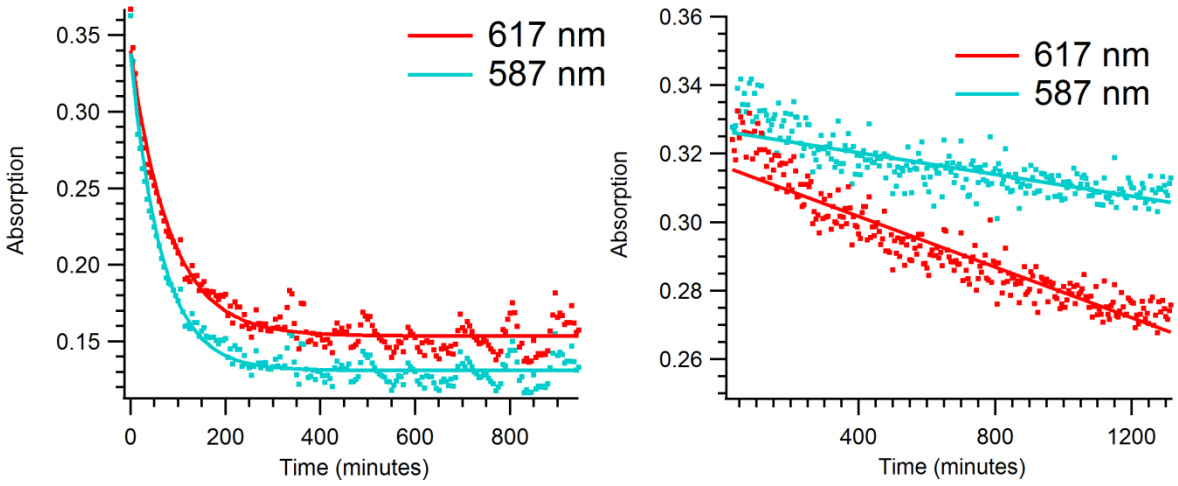

Figure 4.11: Decay rate of water spiked sample (left) and anhydrous ample (right). Observed at wavelengths indicated above.

4.4 Conclusion

An amide cryptand was successfully synthesized and characterized by UV-vis absorption spectroscopy, MCD spectroscopy, EPR spectroscopy, and X-ray diffraction. In an attempt to utilize the complex for small molecule activation or fixation, in particular CO_2 fixation, the product obtained was a solid and completely insoluble in typical laboratory solvents. The only method of characterization performed on the solid was solid state IR spectroscopy. Based upon combined data obtained from a KBr pellet and a nujol mull, it was suggestive that cobalt carbonate was being formed. This is not conclusive evidence however, and future experiments need to be performed to characterize the solid product after bubbling carbon dioxide through a solution of $[Co_2(cryptand_{H\text{-}6})]^{2-}$.

4.5 Future Experiments

The objective of this work was to synthesize a dicobalt cryptand and explore how this complex would interact with biologically relevant small molecules. The product that is formed when carbon dioxide reacts with the cobalt cryptand is largely uncharacterized. It can be definitively stated that whatever reaction might be occurring, it is water sensitive. To further understand the reaction, it is first necessary to find what product is being formed. While IR data suggest that cobalt carbonate could be the product that is being formed, there are two other key experiments that need to be completed to provide supporting evidence. The most powerful tool would be a powder diffraction. This powder diffraction spectrum of the solid can be compared to the published spectrum of cobalt carbonate to give more evidence into what the product is.[28] The last experiment would be elemental analysis. The elemental analysis

would be very useful as the typical elemental analysis is carbon, hydrogen, and nitrogen and with carbonate, the carbon and hydrogen percentages would be expected to be extremely low. To further validate the IR assignments the experiments can be performed in ^{18}O labeled water and CO_2. If the band assigned to the C-O stretch moves to lower energy then it can be assigned as a C-O stretch.

References:

(1) Lopez, N.; Graham, D. J.; McGuire, R.; Alliger, G. E.; Shao-Horn, Y.; Cummins, C. C.; Nocera, D. G. *Science* **2012**, *335*, 450.

(2) Donoghue, P. J.; Gupta, A. K.; Boyce, D. W.; Cramer, C. J.; Tolman, W. B. *Journal of the American Chemical Society* **2010**, *132*, 15869.

(3) Chen, J. M.; Wei, W.; Feng, X. L.; Lu, T. B. *Chemistry-an Asian Journal* **2007**, *2*, 710.

(4) Amendola, V.; Bastianello, E.; Fabbrizzi, L.; Mangano, C.; Pallavicini, P.; Perotti, A.; Lanfredi, A. M.; Ugozzoli, F. *Angewandte Chemie-International Edition* **2000**, *39*, 2917.

(5) Drew, M. G. B.; Hunter, J.; Marrs, D. J.; Nelson, J.; Harding, C. *Journal of the Chemical Society-Dalton Transactions* **1992**, 3235.

(6) Amendola, V.; Fabbrizzi, L.; Mangano, C.; Pallavicini, P.; Poggi, A.; Taglietti, A. *Coordination Chemistry Reviews* **2001**, *219*, 821.

(7) Alberts, A. H.; Annunziata, R.; Lehn, J. M. *J. Am. Chem. Soc.* **1977**, *99*, 8502.

(8) Lehn, J. M. *Pure Appl. Chem.* **1977**, *49*, 857.

(9) Lehn, J. M.; Pine, S. H.; Watanabe, E.; Willard, A. K. *J. Am. Chem. Soc.* **1977**, *99*, 6766.

(10) Lehn, J. M.; Simon, J. *Helv. Chim. Acta* **1977**, *60*, 141.

(11) Motekaitis, R. J.; Martell, A. E.; Lehn, J. M.; Watanabe, E. *Inorg. Chem.* **1982**, *21*, 4253.

(12) Lehn, J. M. *Pure Appl. Chem.* **1978**, *50*, 871.

(13) Lehn, J. M. *Acc. Chem. Res.* **1978**, *11*, 49.

(14) Lehn, J. M. *Pure Appl. Chem.* **1980**, *52*, 2303.

(15) Dietrich, B.; Lehn, J. M.; Sauvage, J. P. *Tetrahedron Lett.* **1969**, 2889.

(16) Dietrich, B.; Academic: 1984; Vol. 2, p 337.

(17) Agnus, Y.; Louis, R.; Weiss, R. *J. Am. Chem. Soc.* **1979**, *101*, 3381.

(18) McKee, V.; Dagdigian, J. V.; Bau, R.; Reed, C. A. *J. Am. Chem. Soc.* **1981**, *103*, 7000.

(19) McKee, V.; Nelson, J.; Town, R. M. *Chemical Society Reviews* **2003**, *32*, 309.

(20) Menif, R.; Reibenspies, J.; Martell, A. E. *Inorganic Chemistry* **1991**, *30*, 3446.

(21) Palmer, D. A.; Vaneldik, R. *Chemical Reviews* **1983**, *83*, 651.

(22) Bolton, J. R. *Science* **1978**, *202*, 705.

(23) Eisenberg, R.; Nocera, D. G. *Inorganic Chemistry* **2005**, *44*, 6799.

(24) Kang, S. O.; VanderVelde, D.; Powell, D.; Bowman-James, K. *Journal of the American Chemical Society* **2004**, *126*, 12272.

(25) Alliger, G. E.; Muller, P.; Cummins, C. C.; Nocera, D. G. *Inorganic Chemistry* **2010**, *49*, 3697.

(26) Alliger, G. E.; Muller, P.; Do, L. H.; Cummins, C. C.; Nocera, D. G. *Inorganic Chemistry* **2011**, *50*, 4107.

(27) Betley, T. A.; Wu, Q.; Van Voorhis, T.; Nocera, D. G. *Inorganic Chemistry* **2008**, *47*, 1849.

(28) Swanson, H. E.; Cook, M. I.; Evans, E. H.; deGroot, J. H. *Natl. Bur. Stand. Circ. (U. S.)* **1960**, *539*, 61 pp.

(29) Li, C. C.; Yin, X. M.; Wang, T. H.; Zeng, H. C. *Chemistry of Materials* **2009**, *21*, 4984.

Experimental

Chapter 5

All reagents and solvents were purchased from vendors and, unless specified, were used without further purification. One liter containers of DMF from Sigma-Aldrich used for anaerobic syntheses were purchased in Sure-Seal containers and bubbled with argon for no less than 30 minutes and stored in an argon glove box. Diethyl ether for use in anaerobic syntheses was dried initially with calcium chloride. The ether was then decanted to a flask containing sodium and benzophenone and refluxed under an argon atmosphere using schlenk techniques. The ether was collected by distillation and underwent three freeze/pump/thaw cycles. Methanol used for anaerobic syntheses was purified by initially putting Mg turning in the bottom of a 2L round bottomed flask then adding solid iodine and heating the flask until iodine coats the turnings. The flask was cooled and methanol was added and refluxed under an argon atmosphere using schlenk techniques. The methanol was collected by distillation and underwent three freeze/pump/thaw cycles to ensure complete removal of oxygen. Conversely, after the purchase of a Pure Solv Micro Solvent Purification System for Innovative Technology Inc., acetonitrile and diethyl ether were purged with argon for 30 minutes passed through an alumina column under an inert atmosphere and used without further purification. Methanol was purged for 30 minutes with argon passed through a DriRite™ column under an inert atmosphere and used without further purification.

$[Cu(CH_3CN)_4]$ OTf

The purification of copper(tetrakisacetonitrile) triflate ($[Cu(CH_3CN)_4]OTf$) was achieved following a published procedure.[1] The purpose of this procedure is to disproportionate Cu(II) and Cu into two moles of Cu(I) to remove any Cu(II) contaminants. In this procedure, which was

performed in an argon-filled glovebox, 2.009 g of copper(tetrakisacetonitrile) triflate, purchased from Sigma-Aldrich, was dissolved in 20 mL of dry, degased acetonitrile. To this solution 0.551 g of copper foil was added and the solution was stirred magnetically for five days. The solution was filtered to remove impurities and the $[Cu(CH_3CN)_4]OTf$ filtrate was collected. 20 mL of ether was added to the entire filtrate and a precipitate formed. The precipitate was collected by filtering with a medium frit and washed three times with ether. The filtrate was discarded. The $[Cu(CH_3CN)_4]OTf$ precipitate was dried and used without further purification. This procedure yielded 2.013 g of $[Cu(CH_3CN)_4]OTf$. Characterization was performed by dissolving 0.058g of recrystallized $[Cu(CH_3CN)_4]OTf$ in 20 mL of water and 25 mL of perchloric acid. This solution was titrated with 1.2 mL of 0.1 M sodium thiosulfate resulting in a color change from yellow to an opaque white mixture.[1] This indicated a Cu(II) contamination of 5 %.

$[Cu(SNS_{Phenyl})Cl]$

The ligand, N^2,N^6-bis(phenyl)pyridine-2,6-dithioicarboxamide (SNS_{Phenyl}), was synthesized following a previously reported procedure.[2] The obtained ^1H NMR assignments are as follows: δ_H (500MHz; DMSO d^6) 12.51 (br, 2H, s), 8.86 (2H, d), 8.25 (1H, t), 7.77 (4H, m), 7.53 (4H, m), 7.39 (2H, m), which are in agreement with the published results.[2] To generate $[Cu(SNS_{Phenyl})Cl]$, 0.0622 g (0.1780 mmol) of SNS_{Phenyl} ligand was placed in 5 mL acetonitrile under normal atmospheric conditions. In a separate vial 0.0260 g copper chloride ($CuCl_2$) (0.1780 mmol) was dissolved in 5 mL acetonitrile. The two solutions were combined and stirred magnetically overnight. The solution was filtered and the green precipitate was collected and recrystallized in DMF by layering with ether. Green needles suitable for X-ray diffraction were grown from

diffusing ether into a solution of 0.030 g [Cu(SNS_{Phenyl})Cl] in 1 mL DMF. Yield 51.2 mg (64.14 %). (m/z: Calc = 446.97; Found = 446.9 $[Cu(SNS_{Phenyl})]^+$). ε_{600}=5000 $M^{-1}cm^{-1}$.

$[Cu(SNS_{t\text{-}butyl})OAc]_2$

The ligand, N^2,N^6-bis(t-butyl)pyridine-2,6-dithiocarboxamide ($SNS_{t\text{-}butyl}$), was synthesized following a previously reported procedure.[3] The obtained ^{1}H NMR assignments are as follows: δ_H (500 MHz; $CDCl_3$) 9.63 (br, 2H, s), 8.88 (2H, d), 7.96 (1H, t), 1.73 (18H, s), which are in agreement with the published results.[3] To generate $[Cu(SNS_{t\text{-}butyl})OAc]_2$, 0.0235 g (0.0759 mmol) of $SNS_{t\text{-}butyl}$ ligand was dissolved in 5 mL acetonitrile. In separate vial, 0.0152 g (0.0761 mmol) of copper acetate monohydrate $[Cu(OAc)_2H_2O]$ was dissolved in 5 mL of acetonitrile under normal atmospheric conditions. The solutions were combined, and immediately turn very dark green. The reaction was allowed to stir magnetically overnight. The solution was filtered with fine frit to remove impurities and solvent was removed under reduced pressure. The product obtained was an oil and was dissolved in 5 mL of dimethyl sulfoxide (DMSO). 5 mL of acetonitrile and 10 mL of hexanes were added to this solution and the solution was placed in a freezer at -20° C. Green needles suitable for X-ray diffraction were formed in the bottom of the vial. Yield 0.0203 g (63.10 %). (m/z: Calc = 407.03; Found = 407.0 $[Cu(SNS_{t\text{-}butyl})Cl]^+$). ε_{930}=1,250 $M^{-1}cm^{-1}$, ε_{450}=7,300 $M^{-1}cm^{-1}$.

$[Cu(SNS_{t\text{-}butyl})Cl]_2$

To generate $[Cu(SNS_{t\text{-}butyl})Cl]_2$, 0.1324 g (0.0428mmol) of $SNS_{t\text{-}butyl}$ ligand was dissolved in 10 mL of acetonitrile under normal atmospheric conditions. In a separate container 0.0575 g (0.0428

mmol) of $CuCl_2$ were dissolved in 10 mL of acetonitrile. The two solutions were combined and immediately a dark green precipitate formed. The solution was allowed to stir magnetically overnight. The precipitate was isolated by suction filtration with a fine frit and the filtrate was discarded. The product was recrystallized by layering a concentrated solution of $[Cu(SNS_{t\text{-}butyl})Cl]_2$ in 1 mL of DMF with 5 mL of ether. Green needle crystals suitable for X-ray diffraction were grown by a 10 mL ether diffusion into a concentrated 1 mL solution of $[Cu(SNS_{t\text{-}butyl})Cl]_2$ in DMF. Yield 0.0145 g (83.18%). (m/z: Calc = 405.02; Found = 405.0 $[Cu(SNS_{t\text{-}butyl\ H\text{-}2})Cl]^-$). ε_{385}=5,000 $M^{-1}cm^{-1}$ ε_{620}=400 $M^{-1}cm^{-1}$. Elemental analysis calculated for $C_{18}H_{30}Cl_4Cu_2N_4OS_2$: C, 33.18; H, 4.64; N, 8.6. Found: C, 32.82; H 4.64; N, 7.51.

Reaction of $[Cu(SNS_{t\text{-}butyl})Cl]_2$ with Triethylamine (Representative Experiment)

A 0.123mM solution of $[Cu(SNS_{t\text{-}butyl})Cl]_2$ was made by massing 0.0050 g of complex and putting the sample into a 100 mL volumetric flask. Acetonitrile was added to the volumetric flask until the solution was diluted to the 100 mL mark. In a separate 100 mL volumetric flask, 100 µL of 7.17 M triethylamine was added and diluted to the mark with acetonitrile producing a 7.17 mM solution of triethylamine. Three mL of the $[Cu(SNS_{t\text{-}butyl})Cl]_2$ solution were placed into a cuvette and the absorption spectrum was taken. To the $[Cu(SNS_{t\text{-}butyl})Cl]_2$ solution, 0.1 equivalents (5.15 µL), of the 7.17 mM triethylamine solution were added and absorption spectra were collected after each addition until a total of four equivalents were added. The same experiments were performed, stopping at 0.7, 0.8, 2.0 and 4.0 equivalents. At these equivalents 300 µL of the sample were taken out of the cuvette and placed in an EPR tube for further analysis. Similar steps were taken when performing the experiment in 7:3 DMF:DMA.

[Cu_2(PyEtAm$_{H-4}$)]

This complex was synthesized according to a previously published procedure.[4] (m/z: Calc = 619.08; Found = 619.3 [Cu_2(PyEtAm$_{H-3}$)]$^+$). ε_{585} = 310 M^{-1} cm^{-1}.

[Cu(PyEtAm$_{H-2}$)]$^-$

The tetramido/diamino macrocyclic ligand, PyEtAm, was synthesized following a previously reported procedure.[5,6] Under an argon atmosphere in a glovebox 0.0250 g (0.504 mmol) of the PyEtAm macrocycle were placed in a scintillation vial. To this 15 mL of DMF were added and the mixture was stirred magnetically. Subsequently 0.040 g (2.016 mmol) of sodium hydride (NaH) (60% w/w in mineral oil) were added to the already stirring ligand solution and allowed to stir for 1 h. To the slurry containing the sodium hydride and ligand, 0.190 g (1.008 mmol) of [$Cu(CH_3CN)_4$]$^+$OTf$^-$ were added. The solution immediately turned green in color, but upon stirring for 12h the solution turned yellow. The precipitated product was filtered and collected. Ether was added to the filtrate to yield more precipitated product. This solution was filtered to collect the precipitatedproduct. The filtrate was discarded and the two solid products combined. The yellow/brown solid was then dissolved in 2 mL of methanol and 10 mL of ether were allowed to diffuse into the methanol solution. Yellow plate crystals were obtained and were suitable for X-ray diffraction (0.206 g, 74%). δ_H (400 MHz; DMSO d_6) 8.92 (br,s, NH_{amide}), 7.56 (4H$_{Pyridine}$, s), 7.34 (2H$_{Pyridine}$, s), 2.39 (8H$_{Ethyl\ linkers}$, s).

$[Cu_2(PyEtAm_{H-4})] + KO_2$ (Typical Reaction)

Preparation of potassium superoxide solutions were performed by addition of 0.0036 g (0.0051mmol) of KO_2 and 0.0360 g (0.1362 mmol) of 18-crown-6 ether into 20mL DMF in a 20 mL scintillation vial. This solution was sonicated for 10 s then magnetically stirred for 15 m. In a UV-vis cuvette, 2.5 mL of the KO_2 solution (5mM) were added and allowed to cool in a cryostat at -40°C for 15 m. This solution was never used more than once, as KO_2 disproportionates rapidly. A stock solution of $[Cu_2(PyEtAm_{H-4})]$ (0.75 mM) in DMF was stirred magnetically for 10 min. 0.5 mL of the of the $[Cu_2(PyEtAm_{H-4})]$ solution was added to the cuvette containing KO_2 in 10 aliquots of 0.05 mL per addition, (over the time period of 10 m) in order to prevent a significant rise in temperature. The spectra changed with absorption bands growing in at 505 nm and 438 nm.

$[Cu_2(NNN_{Phenyl})_2]^{2-}$

The ligand, N^2,N^6-bis(phenyl)pyridine-2,6-dicarboxamide (NNN_{Phenyl}), was synthesized following a previously reported procedure.[7,8] The obtained ^1H NMR assignments are as follows: δ_H (400 MHz; DMSO d^6) 11.05 (NH, 2H, s), 8.41 ($2H_{pyridine}$, d), 8.32 ($4H_{Pyridine}$, t), 7.92 ($4H_{Phenyl}$, d), 7.46 ($4H_{Phenyl}$, t), 7.21 ($2H_{Phenyl}$, t), which are in good agreement with the published spectrum. [7,8] To produce $[Cu_2(NNN_{Phenyl})_2]^{2-}$, in an argon-filled glove box, 0.044 g (0.1388 mmol) of NNN_{Phenyl} ligand were dissolved in 4 mL DMF. While stirring the solution, 0.56 mL (0.28 mmol) of potassium bis(trimethyl)silylamide were added to the solution. To this clear solution 0.052 g (1.380 mmol) of $[Cu(CH_3CN)_4]OTf$ were added and stirred magnetically overnight. The solution

was filtered to remove impurities with a fine frit and the filtrate was collected. Solvent was evaporated under reduced pressure to yield red oil. This oil was redissolved in acetonitrile and recrystallized by layering with toluene. The $[Cu_2(NNN_{Phenyl})_2]^{2-}$precipitate was collected by filtering with a fine frit and the filtrate discarded. 20 mg of this solid were redissolved in 1 mL of DMF and 10 mL of ether were diffused into the solution producing maroon needle shaped crystals suitable for X-ray diffraction. Yield 0.032 g (60.99 %). δ_H (500 MHz; CD_3CN) 7.97 ($2H_{Pyridine}$, d), 7.87 ($1H_{Pyridine}$, t), 7.19 ($4H_{Phenyl}$, d), 6.81 ($4H_{Phenyl}$, t), 6.59 ($2H_{Phenyl}$, t).

$[Co_2(cryptand_{H\text{-}6})]^{2-}$

The ligand, *p*-xylyl cryptand, was synthesized following a previously reported procedure.[9,10] The obtained ^{1}H NMR assignments are as follows: δ_H (500 MHz; DMSO d^6) 7.78 ($6H_{Amide}$, s), 7.30 ($12H_{p\text{-}xylyl}$, s), 4.34 ($12H_{Ethyl\text{-}linker}$, t), 2.51 ($12H_{Ethyl\text{-}linker}$, m), which are in good agreement with the published spectrum.[9,10] To synthesize $[Co_2(cryptand_{H\text{-}6})]^{2-}$, in an argon-filled glove box 0.127 g (0.000186 mmol) of cryptand was placed into 200 mL DMF and stirred producing a white slurry. 2.25 mL (1.13 mmol) of 0.5 M potassium bis(trimethyl)silylamide in toluene were added and the solution became clear. To this solution 0.066 g (0.3725 mmol) of $Co(OAc)_2$ were added and the solution was stirred magnetically for 48 h. The solution was filtered through a fine frit and the solid was collected. The solid $[Co_2(cryptand_{H\text{-}6})]^{2-}$ was redissolved in 50 mL methanol and filtered with a 0.45 µm polytetrafluoroethylene (PTFE) syringe filter. The filtrate was collected and solvent was removed under reduced pressure. Teal block shaped crystals suitable for x-ray diffraction were grown by slow evaporation of methanol. Yield 0.1584 g (63.44%). (m/z: Calc = 795.15; Found = 795.18 $[Co_2(cryptand_{H\text{-}5})]^-$). ε_{587}=140 $M^{-1}cm^{-1}$ ε_{617}=120 $M^{-1}cm^{-1}$.

Magnetic Circular Dichroism Spectroscopy (MCD)

Data were collected using a Jasco circular dichroism spectrometer (J-815) interfaced with an Oxford Instruments magnetocryostat (SM-4000-8) capable of a horizontal field up to 8 T and a temperature range of 1.5 to 300 K.

Preparation of MCD Samples

$[Cu_2(PyEtAm_{H-4})]$

A 2.5 mM solution of $[Cu_2(PyEtAm_{H-4})]$ was formed using 7:3 DMF:DMA as a solvent. The sample was injected into a copper MCD cell with two rubber spacers between two quartz disks. The samples were flash frozen and kept in a liquid nitrogen environment until analyzed. The sample was analyzed at 2 K, 4 K, 8 K, and 15 K. Variable-temperature, variable-field (VTVH) data were also collected at these temperatures while altering the magnetic field in one tesla increments from 7 T to -7 T.

$[Co_2(cryptand_{H-6})]^{2-}$

Mull samples of $[Co_2(cryptand_{H-6})]^{2-}$ were formed by grinding 8.1 mg of $[Co_2(cryptand_{H-6})]^{2-}$ into a fine powder using a mortar and pestle. To this powder, one drop of polydimethylsiloxane (PDMS) was added and the sample was ground with the mortar and pestle until an even dispersion of the $[Co_2(cryptand_{H-6})]^{2-}$ was achieved. The samples were then put between two quartz discs, put between two rubber spacers, and put into a copper MCD cell. The samples

were flash frozen and kept in a liquid nitrogen environment until analyzed. The samples were analyzed at 2 K, 4 K, 8 K, and 15 K. VTVH data were also collected at these temperatures while altering the magnetic field in one tesla increments from 7 T to -7 T.

Electron Paramagnetic Resonance Spectroscopy (EPR)

Data were collected on the samples using an X-band (9 GHz) Bruker EMXPlus spectrometer equipped with an Oxford ESR900 continuous-flow liquid helium cryostat and an Oxford ITC503 temperature system to monitor and regulate the temperature. A dual mode cavity (Bruker ER4116DM) was used for perpendicular mode detection.

Preparation of EPR Samples and Specific Data Collection Parameters

[Cu_2(PyEtAm$_{H-4}$)]

A 0.1mM solution of [Cu_2(PyEtAm$_{H-4}$)] was formed using 7:3 DMF:DMA as a solvent. 300 µL of the copper solution was transferred to a 4mm quartz EPR tube. The sample was flash frozen and kept in a liquid nitrogen environment until analyzed. The sample was analyzed at 5 K under non-saturating conditions with a modulation amplitude of 4 G, a modulation frequency of 100 kHz, and a microwave frequency of 9.637376 GHz.

[Cu_2(SNS$_{t\text{-butyl}}$)$_2$$Cl_2$]

A 0.123 mM solution of [Cu_2(SNS$_{t\text{-butyl}}$)$_2$$Cl_2$] was made by dissolving 0.0050 g of [Cu_2(SNS$_{t\text{-butyl}}$)$_2$$Cl_2$] in 100 mL of acetonitrile. Three mL of this solution were put into a quartz cuvette and

the absorption spectrum was taken. In a separate volumetric flask a 7.17 mM solution of triethylamine was made by putting 100 µL of triethylamine into the flask and diluting it to the mark with acetonitrile. 5.15 µL (0.1 eq) of the diluted triethylamine were added to the cuvette with the metal complex in solution. The absorption spectrum was taken and when the spectrum indicated change to a new species the cuvette was taken out and 300 µL were extracted from the cuvette and placed into a 4 mm quartz EPR tube. This procedure was repeated and aliquots were extracted at 0.7, 0.8, 2.0, and 4.0 equivalents of triethylamine. The samples were flash frozen and stored under liquid nitrogen until analyzed. The samples were analyzed at 5 K with a modulation amplitude of 5 G, a modulation frequency of 100 kHz, and under non-saturating conditions. The samples with 0, 0.7, 0.8, 2.0, and 4.0 equivalents of base had a microwave frequencies of 9.637076, 9.640026, 9.635957, 9.636357, and 9.636937 GHz, respectively.

A similar procedure was followed when adding triethylamine to a solution of $[Cu_2(SNS_{t\text{-}butyl})_2Cl_2]$ in 7:3 DMF:DMA. The difference being that DMF:DMA was used to make the 0.123 mM solution of $[Cu_2(SNS_{t\text{-}butyl})_2Cl_2]$ and DMF:DMA was used in the preparation of the 7.17 mM solution of triethylamine. Another small difference was that the absorption spectrum indicated that a change occurred at 0.4 equivalents not 0.7 equivalents. Under non-saturating conditions, a modulation frequency of 100 kHz, and modulation ampliture 5 G at 5 K the EPR spectra were taken and the microwave frequencies for the 0, 0.4, 1, and 2 equivalents of base were 9.635452, 9.637397, 9.637365, and 9.636456 GHz, respectively.

Electronic Absorption Spectroscopy

Electronic absorption spectra were recorded on a Cary 50 Bio spectrophotometer (Varian) or an Agilent 8453 spectrometer, each of which was interfaced with a Unisoku cryostat (USP-203-A).

^{1}H NMR Spectra

^{1}H NMR spectra were obtained on a Bruker DRX 400 MHz NMR spectrometer or a Bruker DRX 500 NMR spectrometer.

Mass Spectrometry

ESI-mass spectrometry experiments were performed using an LCT Primers MicroMass electrospray-ionization time-of-flight instrument.

X-ray Diffraction

Crystals suitable for x-ray diffraction were analyzed using a Bruker SMART APEX single-crystal diffractometer with a Mo x-ray source, a graphite monochromator, and a SMART APEX (CCD) detector. Alternatively, a Bruker MicroSTAR Cu rotating anode X-ray source with HELIOS or HELIOS PLATINUM 135 CCD detector or an APEX II CCD detector was used. All X-ray data were collected at 100 K.

References:

(1) Irangu, J. K.; Jordan, R. B. *Inorganic Chemistry* **2003**, *42*, 3934.

(2) Begum, R. A.; Powell, D.; Bowman-James, K. *Inorg. Chem.* **2006**, *45*, 964.

(3) Wang, Q.-Q.; Ara, B. R.; Day, V. W.; Bowman-James, K. *Inorg. Chem. (Washington, DC, U. S.)* **2012**, *51*, 760.

(4) Ghosh, S.; Roehm, B.; Begum, R. A.; Kut, J.; Hossain, M. A.; Day, V. W.; Bowman-James, K. *Inorganic Chemistry* **2007**, *46*, 9519.

(5) Hossain, M. A.; Kang, S. O.; Powell, D.; Bowman-James, K. *Inorganic Chemistry* **2003**, *42*, 1397.

(6) Hossain, M. A.; Llinares, J. M.; Powell, D.; Bowman-James, K. *Inorganic Chemistry* **2001**, *40*, 2936.

(7) Banihashemi, A.; Eghbali, M. *J. Polym. Sci., Polym. Chem. Ed.* **1976**, *14*, 2659.

(8) Brzozka, Z. *Analyst (London)* **1988**, *113*, 891.

(9) Kang, S. O.; Llinares, J. M.; Powell, D.; VanderVelde, D.; Bowman-James, K. *Journal of the American Chemical Society* **2003**, *125*, 10152.

(10) Kang, S. O.; VanderVelde, D.; Powell, D.; Bowman-James, K. *Journal of the American Chemical Society* **2004**, *126*, 12272.